UNIVERSIDADE DE LISBOA
FACULDADE DE CIÊNCIAS
DEPARTAMENTO DE FÍSICA

Robustness of photon dose distributions against intra and inter-fraction anatomical changes for whole lung irradiation

Mariana Silva Pereira Fialho da Piedade

Mestrado Integrado em Engenharia Biomédica e Biofísica
Perfil em Radiações em Diagnóstico e Terapia

Dissertação orientada por:
Dr. Enrica Seravalli
Prof. Dr. Raquel Conceição

2022

Acknowledgements

2021 was, without a doubt, a challenging year. The unpredictability of the course of the COVID-19 pandemic was not easy to deal with, and the uncertainty I experienced certainly had an impact on how I lived this chapter of my life. However, I am grateful to have been able to carry out my project, even with all its delays and setbacks, and to have lived an amazing time. Thus, some acknowledgements are in order.

Firstly, I would like to express my deepest gratitude to my supervisor, Enrica Seravalli who made this project possible and always provided me with guidance and support. Enrica always made sure I felt welcome and motivated during the course of the project. Also, her availability was always perfect, with quick emails and meetings every time they were needed. For that I am very thankful.

I would like to thank everyone at the UMCU that took some of their time to help me with this project and without their help I could not have done it, namely Cornel Zachiu, Gijs Bol, Mirjam Willemsen-Bosman and Sarah Hackett. I would also like to express my gratitude to Filipa Guerreiro, for being so friendly to a random girl approaching her to ask about her work and for all the help during the time she worked at the UMCU.

I wish to express my gratitude to Professora Raquel Conceição for all the support before and during my thesis project, for the availability to always help in any way she could and for the regular meetings that often turned into nice conversations.

I wish to express my acknowledgements to the Erasmus+ program for allowing me this opportunity.

To my friends from the Biltstraat house and the others spread around Utrecht and the Netherlands, I want to thank for making this stay so amazing. Even when everything was closed and lockdown rules were in place, I never felt alone. To my friends either from FCUL or back home, I am very grateful for their friendship throughout all these years, for being there in my better and worst moments. Thanks for the dinners, beers, parties, study sessions and coffee breaks. A special acknowledgment goes to my friends Bárbara, Mariana, Soraia and Rute, for simply being the best girl group in the world.

I very special thank you goes to Peter, for being so supportive, patient and for making me happy every day. You were a great part of this experience and I am very grateful to have been able to live it with you. Even though you made me walk on ice.

Lastly, I would like to express my very profound gratitude to my family. They were always there for me growing up and made me who I am today. A special thank you goes to my parents and brother for always supporting me and for encouraging me to pursue what made me happy. I could never have accomplished this without them. Thank you for everything.

Abstract

Approximately 400 000 children are diagnosed with cancer every year, with the most common types of childhood cancers being leukemia, lymphoma, brain and solid tumors. Moreover, 10-40% of children with solid tumors present lung metastases at the time of diagnosis.

Whole lung irradiation (WLI) is a treatment option for pediatric patients with lung metastases that develop from solid tumors like Ewing's sarcoma (ES), rhabdomyosarcoma, and Wilms' tumor (WT). However, during treatment delivery, intra and inter-fraction anatomical changes might occur and can greatly affect treatment outcome. These changes can either cause underdosages of the target volume, or overdosage of surrounding organs at risk (OARs). Since growing lung tissue is more sensitive to radiation, avoiding the irradiation of OARs while maintaining target coverage is of utmost importance. Thus, there is the need to ensure that a treatment plan is robust, which is accomplished if the planned and delivery dose distributions agree even in the presence of uncertainties. To evaluate how anatomical changes affect the treatment outcome when delivering WLI to pediatric patients, this thesis comprises a study of robustness of photon dose distributions against intra and inter-fraction anatomical changes.

The present study includes treatment plans of 21 pediatric patients that received WLI at University Medical Center Utrecht. The robustness evaluation was performed against intra and inter-fraction anatomical changes. Intra-fraction changes were evaluated by recalculating the original plan on the two extreme breathing phases – maximum inhalation and maximum exhalation. Conversely, inter-fraction changes were evaluated by calculating the fractional dose on the daily cone-beam computed tomography (CBCT) images acquired before treatment and accumulating the resulting dose distributions. The recalculated plans were then compared to the original dose distribution.

Overall results of the study demonstrated no clinically relevant differences in terms of mean internal target volume (ITV) coverage of the lungs. However, hot spot values differed significantly for three patients. The differences observed for the $V_{107\%}$ were due to diaphragm position shifts (two patients) and electron density (ED) changes within the lung ITV (one patient).

Coverage and hot spots of metastases presented clinically relevant differences when considering the extreme breathing phases, as well as the registered-CTs. This was due to differences in ED within the metastases and position variations in relation to surrounding structures (like the heart or ribs). However, these changes were observed for the PTV only, while ITV coverage remained around 100% on all plans.

OAR dose values were robust against intra and inter-fraction anatomical changes, with no clinically relevant differences to report.

In conclusion, the recalculated WLI plans are considered robust against intra and inter-fraction anatomical changes when taking into consideration average results. However, some clinically relevant differences were identified per patient, which require further attention and improvement in future treatment plans.

Key words: Whole lung irradiation, photon therapy, intra-fraction anatomical changes, inter-fraction anatomical changes.

Resumo

O conceito de radioterapia tem por base a utilização de radiação ionizante para erradicar células tumorais ao promover a morte celular (Minniti et al., 2012). O efeito biológico produzido pela radiação ionizante é quantificado pela quantidade de radiação absorvida por unidade de massa, sendo a unidade SI para dose absorvida o Gray (Gy) (Khan, 2003). Os efeitos da radiação diferem entre adultos e crianças, sendo a população pediátrica mais sensível à radiação. Isto deve-se ao facto de as crianças apresentarem tecidos ainda em desenvolvimento, contrariamente aos dos adultos (Paulino et al., 2000).

Todos os anos, aproximadamente 400 000 crianças são diagnosticadas com cancro, sendo os tipos mais comuns de cancro pediátrico a leucemia, linfoma, tumores cerebrais e tumores sólidos (Steliarova-Foucher et al., 2017). Além disso, 10-40% das crianças com tumores sólidos apresentam metástases pulmonares no momento do diagnóstico, com taxas de sobrevivência entre os 20 e os 70% (Fuchs et al., 2012). Apesar da taxa de sobrevivência ter aumentado nos últimos anos, principalmente devido ao desenvolvimento de novas técnicas de radioterapia, um novo problema surge na população sobrevivente: a posterior toxicidade provocada pela radiação (Paulino et al., 2000). Nos casos em que a radiação incide sobre os pulmões, o risco de complicações a longo prazo nos pulmões, coração, glândulas mamárias e tiroide é considerável. Mais concretamente, estudos com doentes submetidos a irradiação do pulmão demonstram casos de fibrose pulmonar, pneumonia recorrente, falta de ar, desenvolvimento anormal do tórax, insuficiência cardíaca, enfarte do miocárdio, doença pericárdica, hipotiroidismo, hipoplasia mamária e cancros secundários (Mertens et al., 2002; Kalapurakal, Lee, et al., 2019; Lange et al., 2014).

A irradiação total do pulmão (*whole lung irradiation, WLI*) é uma opção de tratamento para doentes pediátricos com metástases pulmonares que se desenvolvem a partir de tumores sólidos, tais como sarcoma de Ewing, rabdomiossarcoma e tumor de Wilms (Paulino et al., 2000). No entanto, durante o tratamento podem ocorrer alterações anatómicas. Estas alterações podem ocorrer durante uma só fração, denominando-se intrafração, ou entre frações do tratamento, denominando-se interfração, e podem provocar uma subdosagem do volume alvo ou sobredosagem de órgãos em risco (*organs at risk, OAR*) adjacentes (Van Herk, 2004). Desta forma, evitar a irradiação de órgãos críticos mantendo a cobertura do volume alvo é de extrema importância. No contexto de planeamento de radioterapia, existem vários volumes-alvo a considerar, dos quais os mais relevantes são o volume alvo interno (*internal target volume, ITV*), que é definido ao expandir o volume tumoral por uma margem personalizada para cada doente, que tem em conta a amplitude do movimento respiratório (Ichiji et al., 2013); e o volume alvo de planeamento (*planning target volume, PTV*), que é o resultado de uma expansão do ITV por uma determinada margem, sendo esta específica da instituição considerada (Purdy, 2004). Estas margens são criadas com o objetivo de fazer face à presença de incertezas, sendo que o ITV deve assegurar a correta irradiação do pulmão na presença de incertezas causadas, por exemplo, pelo movimento respiratório, enquanto o PTV deve assegurar o tratamento na presença de incertezas causadas por, por exemplo, erros de posicionamento. Assim, há a necessidade de garantir que um plano de tratamento é robusto, o que é concretizado se a dose planeada e a dose que está a ser administrada ao doente coincidirem, mesmo

na presença de incertezas (Albertini et al., 2011). Para avaliar de que forma as alterações anatómicas afetam a administração de radiação total do pulmão a doentes pediátricos, esta dissertação compreende um estudo de robustez tendo em conta alterações anatómicas intra e interfração.

O presente estudo inclui planos de tratamento de 21 doentes pediátricos que receberam WLI no University Medical Center Utrecht. Os doentes incluídos neste estudo apresentam uma média de 7 anos de idade aquando do tratamento e tumor de Wilms, sarcoma de Ewing, tumor rabdoide, sarcoma epitelial e sarcoma sinovial como tumores primários. Para todos os doentes, o tratamento foi administrado recorrendo à técnica de arcoterapia volumétrica modulada (*volumetric-modulated arc therapy, VMAT*). Nesta técnica, a gantry (braço do acelerador linear do qual são emitidos os feixes de fotões) roda à volta do doente, varrendo um ângulo de 360º (Teoh et al., 2011). Adicionalmente, os doentes foram divididos em dois grupos — doentes sem e doentes com metástases pulmonares. Esta divisão foi efetuada com base nas diferentes distribuições de dose esperadas para estes dois grupos, já que um doente que recebe dose primária e *boosts* localizadas apresenta uma distribuição de dose muito mais heterogénea do que um doente que recebe apenas uma dose primária. Os doentes sem metástases pulmonares receberam uma dose de 15 Gy em 10 frações (com a exceção de um doente, que recebeu 10.8 Gy em seis frações), enquanto que a maioria dos doentes com metástases receberam doses primária e de reforço de 12 e 22 Gy, respetivamente, em oito frações.

A avaliação de robustez na presença de alterações anatómicas por intrafração foi concretizada ao recalcular o plano original nas duas fases extremas do ciclo respiratório — inspiração e expiração máximas. Na preparação para o tratamento, os doentes realizam uma tomografia computorizada (*computed tomography, CT*) de planeamento, na qual as delineações dos volumes alvo e OARs são efetuadas. Estas CT são divididas em dez fases, representando um ciclo respiratório completo. As fases extremas do ciclo respiratório foram selecionadas por inspeção visual do ciclo de cada doente. Por outro lado, as alterações interfração foram avaliadas calculando a dose fracionada nas imagens diárias de tomografia computorizada de feixe cónico (*cone-beam computed tomography, CBCT*) adquiridas antes do tratamento e acumulando as distribuições de dose resultantes. Os planos recalculados foram comparados com as distribuições de dose originais e foram considerados robustos nos casos em que as diferenças de cobertura são inferiores a 5% para o ITV e PTV dos pulmões e metástases, enquanto as diferenças superiores a 3 Gy foram consideradas clinicamente relevantes para os OARs.

Os resultados do estudo demonstraram que não existem diferenças clinicamente relevantes em termos de dose média absorvida pelos pulmões, bem como na dose média absorvida por OARs adjacentes. No entanto, os resultados por doente revelaram algumas diferenças clinicamente relevantes, principalmente em termos de dose absorvida no ITV dos pulmões e PTV de metástases, que levaram a casos de sub e sobredosagem. Além disso, foram observadas situações de sobredosagem, mesmo no plano original. As causas de sobredosagem foram principalmente associadas a alterações na densidade eletrónica abrangendo todo o pulmão e metástases, mas também ao número de metástases, posicionamento de metástases em relação a OARs e diferença entre a dose primária e a dose de reforço. No entanto, enquanto o PTV das metástases se demonstrou sensível a alterações, o ITV manteve a cobertura necessária tanto nos planos recalculados nas fases extremas do ciclo respiratório, bem como nos planos recalculados nas CBCTs e acumulados.

Em conclusão, os planos de irradiação total do pulmão recalculados são considerados robustos tendo em conta alterações anatómicas por intra e interfração, quando considerada a média dos resultados. No entanto, avaliando os resultados por doente, foram detetadas algumas diferenças clinicamente relevantes. Estas diferenças requerem maior atenção e uma melhoria nos planos de tratamento futuros, através da aplicação de técnicas complementares, tal como a administração da dose com o doente a

suster a respiração ou durante um intervalo específico de forma que a irradiação aconteça numa fase específica do ciclo respiratório (C. Demoor-Goldschmidt et al., 2017; Gorgisyan et al., 2017). Uma outra opção é a utilização de feixes de protões, em vez de fotões, que devido às suas propriedades físicas oferecem uma deposição de dose mais localizada, com menos dose de entrada e saída (que é característica dos fotões) (Mohan et al., 2017). No entanto, a radioterapia com protões apresenta algumas limitações, sendo a sua sensibilidade a alterações no meio a principal. Estas alterações podem facilmente deslocar a deposição da dose e originar uma subdosagem do alvo e sobredosagem de tecido saudável ou OARs circundantes. Por estas razões, a utilização de radioterapia de protões em WLI deve ser bem estudada, com uma necessidade acrescida de estudos de sobrevivência e qualidade de vida a longo-prazo.

Palavras-chave: Irradiação total do pulmão, radioterapia de fotões, alterações anatómicas por intrafração, alterações anatómicas por interfração.

Contents

List of Figures

List of Tables

List of Acronyms

3D Three-dimensional

3D-CT Three-dimensional Computed Tomography

4D Four-dimensional

4D-CT Four-dimensional Computed Tomography

4D-MRI Four-dimensional Magnetic Resonance Imaging

4D-PET Four-dimensional Positron Emission Tomography

CBCT Cone-Beam Computed Tomography

CT Computed Tomography

CTV Clinical Target Volume

$D_{2\%}$ Near maximum dose

D_{mean} Mean dose

DVH Dose-Volume Histogram

ED Electron density

ES Ewing sarcoma

GTV Gross Tumor Volume

Gy Gray

HU Hounsfield Unit

IGRT Image-Guided Radiation Therapy

IMPT Intensity-Modulated Proton Therapy

IMRT Intensity-Modulated Radiation Therapy

IP-AP/PA Inverse-Planned anteroposterior-posteroanterior

ITV Internal Target Volume

kV Kilovolt

kV-CBCT Kilovoltage Cone Beam Computed Tomography

Linac Linear accelerator

MRI Magnetic Resonance Imaging

MV Megavolt

MV-CBCT Megavoltage Cone Beam Computed Tomography

OAR Organ at Risk

PD Prescribed dose

PTV Planning Target Volume

S-AP/PA Standard anteroposterior-posteroanterior

SIB Simultaneous Integrated Boost

SIOP International Society of Pediatric Oncology

SOBP Spread Out Bragg Peak

$\mathbf{V}_{107\%}$ Volume receiving 107% of the prescribed dose

$\mathbf{V}_{21.6Gy}$ Volume receiving 21.6 Gy

$\mathbf{V}_{95\%}$ Volume receiving 95% of the prescribed dose

VMAT Volumetric-Modulated Arc Therapy

WLI Whole Lung Irradiation

WT Wilms' tumor

Chapter 1

Introduction

1.1 Motivation

Each year, approximately 400 000 pediatric patients are diagnosed with cancer, with the most common types of childhood cancers being leukemia, lymphoma, brain and solid tumors, such as neuroblastoma and Wilms' tumor (Steliarova-Foucher et al., 2017). Unlike cancer in adults, the likelihood of childhood cancer arising from external risk factors (apart from previous chemotherapy treatment or exposure to high-dose radiation) is quite low. Thus, most types of cancer in children arise from inherent risk factors, which include birth weight, parental age, and congenital anomalies (Spector et al., 2015).

The outcome of childhood cancer has improved significantly over the past decades, with a current overall survival rate for nonmetastatic pediatric solid tumors between 75-90%. However, 10-40% of children with solid tumors present lung metastases at the time of diagnosis, with survival ranging from 20 to 70%, depending on prognostic factors such as histology and response to chemotherapy. Additionally, surgery, radiotherapy, or both combined, are options to treat metastases that persist after the initial treatment (Fuchs et al., 2012).

Whole Lung Irradiation (WLI) is an option to treat lung metastases that develop from solid tumors such as Ewing's sarcoma, rhabdomyosarcoma, and Wilms' tumor. Focusing on Wilms' tumor patients, there has been great improvement in the patient survival rate over the last four decades and, due to multimodality treatments comprising WLI, the survival outcome is approximately 90% (Paulino et al., 2000).

During radiotherapy treatments, intra and inter-fraction patient anatomical changes might occur. These can be caused by several factors, such as breathing motion or weight changes, and might greatly affect the treatment outcome (Van Herk, 2004). Thus, a radiotherapy plan is considered robust if the planned and delivered dose distributions agree, even in the presence of treatment uncertainties (Albertini et al., 2011).

1.2 Objectives

To better understand how anatomical changes might affect the treatment outcome when delivering WLI to pediatric patients, an evaluation of robustness of the dose distributions needs to be performed. Thus, the aim of the present study is to recalculate existing photon treatment plans of WLI to assess the robustness of the dose distribution against intra-fraction anatomical changes and inter-fraction anatomical changes. This assessment is performed in terms of coverage and hot spots of the target (considered in this study as both lungs and lung metastases) and dose being delivered to the surrounding OARs.

1.3 Thesis Outline

This document is divided in 6 chapters. The theoretical background necessary to understand this work is introduced in Chapter 2, including basic radiotherapy concepts, whole lung irradiation in children, basics of photon therapy and treatment techniques (more precisely techniques used to deliver whole lung irradiation), treatment robustness concepts and imaging techniques relevant to the project. Chapter 3 includes Materials and Methods and, in this chapter, the procedure followed to recalculate the photon treatment plans is detailed. The results of the study are presented and discussed in Chapter 4. Chapter 5 comprises a brief overview of proton therapy concepts, proton therapy techniques to deliver WLI and treatment planning robustness, as well as an introduction to follow-up work towards a comparison study between photon and proton dose distributions against inter-fraction anatomical changes. General conclusions are provided in Chapter 6.

Chapter 2

Background

2.1 Whole lung irradiation in children

With a significant survival rate among Wilms' tumor patients that present lung metastases, the problem of late toxicity that arises from treatment has become increasingly important to tackle, since growing lung tissue is more sensitive to radiation (Paulino et al., 2000). The Childhood Cancer Survival Study showed that 5-year survivors that received chest or whole body irradiation presented an increased risk of long-term pulmonary complications, such as lung fibrosis, a need for supplemental oxygen, recurrent pneumonia, chronic cough, shortness of breath, and abnormal chest wall development (Mertens et al., 2002). Further studies have been conducted regarding the effect of WLI in long-term changes in pulmonary function, revealing that pediatric patients that receive WLI present abnormal pulmonary function tests parameters. These findings suggest that WLI leads to restrictive pulmonary defects, as well as impairments in diffusion capacity (Motosue et al., 2012).

In addition to considering the late toxicity that affects the lungs, it is also necessary to consider other OARs, like the heart. Many reports have shown that WLI, as well as WLI combined with chemotherapy, has led to a higher prevalence of cardiac complications, including congestive heart failure, myocardial infarction, pericardial disease, and valvular heart disease (Kalapurakal, Zhang, et al., 2013). Further studies have been conducted to reduce radiation exposure in other normal tissues, such as the thyroid gland and breast tissues, without compromising lung dose coverage and cardiac protection. The sparing of the thyroid gland and breast tissues is also of importance for later toxicity, since their irradiation might lead to hypothyroidism, breast hypoplasia, and secondary malignant neoplasms (including breast cancer and thyroid cancer) (Kalapurakal, Lee, et al., 2019; Lange et al., 2014).

2.2 Radiotherapy and its application in whole lung irradiation

Radiotherapy refers to the use of ionizing radiation to eradicate tumor cells by means of DNA damage and, consequently, cell death. Although radiation causes equal damage in normal and cancer cells, normal cells repair themselves at a faster rate than cancer cells, which allows them to recover from radiation damage between fractions (Minniti et al., 2012). The SI unit for absorbed dose is Gray (Gy), which is the amount of absorbed radiation energy per unit mass, and quantifies the biologically significant effects produced by ionizing radiation (Khan, 2003).

There are two ways to deliver radiation in radiotherapy treatments: internal and external beam radiotherapy. In internal beam radiotherapy, or brachytherapy, the radiation is delivered from inside the body by placing the radiation source near or in the tumor itself. Conversely, in external beam radiotherapy

the radiation is delivered from outside the body by means of X-ray photons or charged particles (such as protons) (Baskar et al., 2012).

Since children are more sensitive to radiation-induced adverse effects, mainly due to their growing tissues, radiotherapy techniques have evolved to spare normal tissue. Imaging techniques such as X-ray, computed tomography (CT) or magnetic resonance imaging (MRI) are used to increase precision in treatment planning and daily treatment delivery, allowing image-guided radiation therapy (IGRT). The improvement of such imaging techniques during treatment delivery allowed adjusting the radiotherapy fields to the actual tumor volume, and the ability to better identify and define normal tissue to be protected, as well as OARs (Steinmeier et al., 2019).

2.2.1 Physics of photon therapy

X-ray photons are the most widely used form of radiation in radiotherapy treatment. X-rays are produced in a linear accelerator (linac) by sending accelerated electrons against a material with high atomic number. While a photon beam propagating through vacuum is dictated by the inverse square law (the photon energy is inversely proportional to the square of the distance from the radiation source), a photon beam propagating through a patient is affected not only by the inverse square law, but also by the attenuation and scattering of the photon beam inside the patient. The type of interaction the photons undergo in the body depends on the photon energy (see Figure 2.1) and are the following: photoelectric effect, Compton effect and pair production.

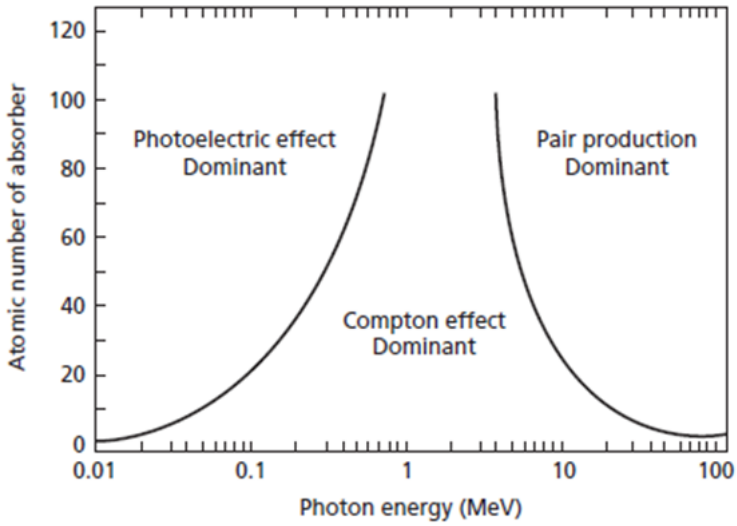

Figure 2.1: Relative importance of the three main types of photon interactions with matter *[adapted from (Hendee et al., 2005)]*.

In the radiotherapy setting, the photon energies range from 6-20 megavolt (MV). For this range of photon energy, the predominant type of radiation interaction with matter is the Compton effect. In the Compton effect, a photon interacts with an orbital electron, transferring part of its energy. The electron is then ejected from the atom as a recoil electron and a scattered photon is produced. Recoil electrons deposit their kinetic energy in the patient, resulting in a dose buildup region between the surface of the patient and the depth at which the dose reaches its maximum value (Podgorsak, 2005), as can be observed in Figure 2.2:

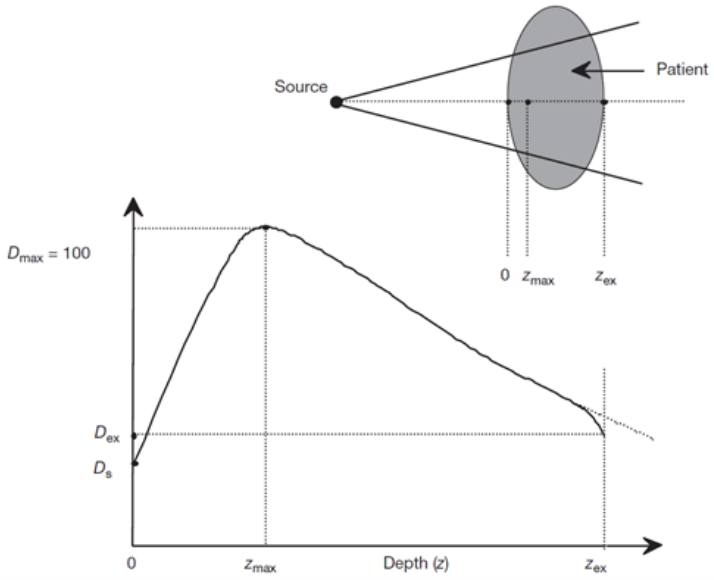

Figure 2.2: Dose deposition of a radiotherapy photon beam in a patient, in which D_s is the dose at the surface of the patient, D_{ex} is the exit dose and D_{max} is the maximum dose. The dose buildup region comprises the distance between $z = 0$ and $z = z_{max}$ *[adapted from (Podgorsak, 2005)]*.

2.2.2 Photon therapy for whole lung irradiation

Concerning techniques to deliver whole lung irradiation, studies (Bosarge et al., 2016; Kalapurakal, Zhang, et al., 2013) have been conducted to compare the most effective treatment approach regarding target coverage as well as normal tissue sparing.

2.2.2.1 Standard technique

The standard technique to deliver whole lung irradiation is anteroposterior-posteroanterior (S-AP/PA) radiotherapy, which is a form of conventional radiotherapy using two opposing fields (Bosarge et al., 2016). In conformal radiotherapy, the radiation beams are shaped to match the target volume and to spare the surrounding normal tissues, allowing a more conformal dose distribution. However, the normal tissues still receive a significant amount of radiation dose and, although conformal radiotherapy is the standard procedure, newer techniques have been developed to deal with its limitations.

2.2.2.2 Intensity-modulated radiotherapy

Intensity-modulated radiotherapy (IMRT) is an advanced form of conformal radiotherapy of particular value for target volumes in close proximity to radiosensitive normal structures. The main differentiation factor of IMRT is the division of the radiation beam into beamlets, each beamlet with a different photon intensity. Additionally, the use of inverse planning in IMRT allows the achievement of optimal intensity across each beamlet, producing a very specific dose distribution — inverse planning specifies the plan outcome in terms of tumor dose and safety margins, and uses a computer system to adjust the beam intensities to find a configuration best matched to the desired plan (Taylor et al., 2004). In this treatment technique, changes are made in the intensity of each beamlet, based on the initial dose distribution, and this process is repeated through several iterations until no other improvement is observed and an optimal dose distribution is achieved (Taylor et al., 2004).

2.2.2.3 Volumetric modulated arc therapy

Another state-of-the-art technique to deliver radiotherapy is volumetric-modulated arc therapy (VMAT). This is a form of arc therapy and consists of a dose delivered by means of a continuous rotation of the radiation source, allowing the patient to be treated from a full 360º beam angle. It is a technique characterized by the simultaneous variation of three parameters: gantry rotation speed, treatment aperture shape and dose rate (Teoh et al., 2011). The variation of these parameters allows more conformal dose distributions, providing a highly conformal treatment combined with adequate sparing of OARs. Compared to IMRT, VMAT has the potential to improve target coverage, dose to the OARs and dose homogeneity. Since it presents a shorter delivery time and requires less monitor units, VMAT allows a reduction in the integral dose to the body. Additionally, the decrease in delivery time not only results in better patient compliance, but also in a lower range of intra-fraction motion, with fewer setup errors (Johnston et al., 2011; Leoncini et al., 2014).

2.3 Treatment planning

2.3.1 Target volume definition and prescribed dose

There are four volumes involved in radiotherapy treatment planning, as seen in Figure 2.3. The first volume to be defined is the Gross Tumor Volume (GTV) and consists of the tumor volume itself. The second one is the Clinical Target Volume (CTV) and it is an expansion of the GTV to account for suspected microscopic disease that is not detected with current imaging techniques (Purdy, 2004). The third one is the Internal Target Volume (ITV) and includes an internal margin determined by the intra-fraction organ motion (Ichiji et al., 2013). The fourth is the Planning Target Volume (PTV) and is an expansion of the ITV by a margin to account for patient setup variations (Purdy, 2004).

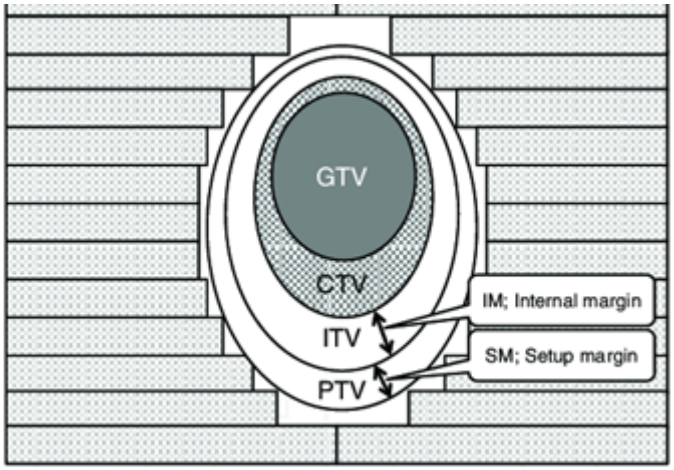

Figure 2.3: Relationship between tumour volumes: Gross Tumor Volume, Clinical Target Volume, Internal Target Volume and Planning Target Volume *[adapted from (Ichiji et al., 2013)]*.

When performing WLI, the CTV is defined as the entire lung volume. To account for intra-fractional motion of the target volume due to respiration, the use of ITV has been introduced, specific for each patient (Ichiji et al., 2013). A new treatment planning guideline was introduced by (Kalapurakal, Lee, et al., 2019), which required the creation of a maximum lung expansion planning volume. This volume was obtained by expanding the ITV by 5 mm in all directions, creating a PTV.

The recommended dose to deliver to children undergoing WLI is between 12 and 15 Gy. The current

practice for Wilms' tumor patients is the administration of 12 Gy in eight fractions (Nicolin et al., 2008), with a 6 MV X-ray beam.

2.3.2 Organs at risk

Regarding OAR contouring, the literature has conflicting studies, with the heart being the only structure that is consensual to spare across all WLI studies. For example, in photon therapy studies, Bosarge et al. considered the esophagus, spinal canal, spleen, stomach and the pericardium as organs to spare (Bosarge et al., 2016). Kalapurakal et al. considered the liver and thyroid gland as organs to spare when using three-dimensional (3D) scans and other heart structures, such as the right and left coronaries and left ventricular myocardium, when using respiration-gated four-dimensional (4D) scans (Kalapurakal, Zhang, et al., 2013). In proton therapy studies, Sha et al. considered the esophagus, liver, spinal cord, vertebrae, humerus and heart, while Wong et al. focused mainly on the dosimetric sparing of the breasts and heart (Sha et al., 2021; Wong et al., 2021).

2.4 Dose distribution robustness

2.4.1 Uncertainties in radiotherapy

In radiotherapy treatment planning and delivery, there are many uncertainties to be considered. Firstly, there are uncertainties in the delineation process, which are systematic and will influence all treatment fractions in an identical way. These can be caused by the limited resolution of imaging modalities, observer "noise" (the same observer, when asked to delineate a target volume twice, will not do it the same way), inter-observer variability in the target definition and differences between image modalities used for treatment planning and dose delivery verification. Secondly, there are uncertainties due to patient setup errors. These can be systematic and random and are caused by positioning variation, which can happen during delivery (intra-fraction changes) or in between fractions (inter-fraction changes). To account for these variations, and to guarantee sufficient target coverage, safety margins are included in treatment planning. Thirdly, there are uncertainties due to anatomical changes, which can be systematic and random. Uncertainties due to anatomical changes include displacements of the target volume and OAR. The displacement of OAR can be caused both by intra-fraction changes (in the case of WLI, the respiration movement is an important factor to consider since the breathing cycle has a time scale shorter than the delivery time of a single fraction) or by inter-fraction changes, such as weight changes (Van Herk, 2004).

The effect of systematic and random errors on the dose distribution is different. Systematic errors will result in a shift of the cumulative dose distribution relative to the target, while random errors will blur the dose distribution (Van Herk, 2004).

2.4.2 Robust radiotherapy planning

The aim of treatment planning is to create plans that are robust against uncertainty. The robustness of a treatment plan refers to two properties: the CTV should receive the prescribed dose (PD) and normal tissue constraints should be satisfied. After defining the CTV, safety margins are added to account for setup and motion-related uncertainties by creating the PTV. It is assumed that, as long as the CTV moves only within the boundaries of the PTV, the PD is being delivered to the CTV. There are specific cases in which the sparing of OAR is of high importance — in the case of WLI, the dose delivered to the heart is

an important concern. In such cases, respecting dose constraints to normal tissue might be given priority over CTV coverage (Unkelbach et al., 2018) and a planning risk volume is created by contouring normal tissue and expanding it by a given margin (Burnet et al., 2018; Unkelbach et al., 2018).

There are a few limitations regarding the PTV concept. One limitation includes the fact that it relies on the assumption that the dose distribution is unaffected by changes in the patient's anatomy, which is unrealistic to assume. Another limitation to consider is that the CTV might not receive the PD. This depends more on the dose distribution than on the geometric margin concept. Since dose distributions are not perfectly conformal to the PTV and are not equally conformal on all sides of the CTV, the optimal margin can therefore be anisotropic (different margins in different directions from the CTV). Due to these limitations, robust planning methods that incorporate uncertainty into treatment plan optimization for IMRT and intensity-modulated proton therapy (IMPT) have been developed (Unkelbach et al., 2018).

To face the uncertainty that arises from the breathing motion, the concept of an internal target volume ITV was introduced (Ichiji et al., 2013). As mentioned in the previous section "Photon therapy for whole lung irradiation", this volume accounts for uncertainties that arise from the breathing motion and is individual for each patient. A safety margin is then added to the ITV which, based on the literature regarding current WLI treatment guidelines, is 5 mm (Kalapurakal, Lee, et al., 2019).

2.4.3 Image-guided radiotherapy

Large safety margins lead to robust plans that ensure adequate target coverage in case large errors occur, but also imply the irradiation of considerable volumes of normal tissues (Cho et al., 2002). The use of IGRT allows to reduce geometrical uncertainties within treatment delivery, and, by reducing such uncertainties, to reduce the safety margins (Court, 2014).

CBCT allows to visualize the target volume in relation to OAR and assess intra and inter-fraction uncertainties, making a correction in alignment of the target volume in relation to the radiotherapy beam. These CBCT images are acquired daily before each fraction throughout the whole treatment and allow an evaluation of the delivered dose, followed by the implementation of adaptative strategies in case of underdosage (Kranen et al., 2016).

2.5 Medical imaging modalities in radiotherapy

In the last two decades, imaging, planning and delivery technology have progressed in a way that it is now possible to consider a 4D model of the patient, consisting of three spatial dimensions and time as a fourth dimension. This contrasts from the previous model of the patient undergoing radiotherapy, which was assumed to be static over the course of the treatment. Imaging moving anatomy may result in the presence of artifacts in the reconstructed image, which can lead to incorrect object position, shape and size in the image, blurring or distortion of the object boundary, decrease in contrast resolution and increased image noise (Hugo et al., 2012).

At first, techniques to deal with image artifacts were introduced in cardiac imaging (to address the beating heart) (Kachelriess et al., 2000) and later were transferred to the entire thorax to deal with respiration. However, the initial intent of these methods was to suppress motion and artifact to produce a clear image of the patient for diagnostic applications only. For diagnosis purposes, the motion range and direction in which anatomy is moving are not important and therefore are not measured. For radiotherapy purposes, the motion pattern impacts the dose that is being delivered to the patient and so it is necessary to collect more information regarding the motion to create a robust treatment plan. To face this

need, 4D imaging techniques were developed specifically for radiotherapy applications. Since CT is the main imaging modality for radiotherapy planning and used in IGRT, it was the first imaging modality to incorporate time as a fourth dimension. This was quickly followed by 4D-MRI, 4D CBCT and 4D positron emission tomography (PET) (Hugo et al., 2012).

2.5.1 4D computed tomography

CT has been evolving since the first generation scanner developed in 1972 (Ambrose et al., 1973). Almost 20 years after, slip ring technology — an electromagnetic apparatus that allows electrical signals to be transmitted from a stationary to a rotating structure, enabling a continuous gantry rotation and resulting in a helical scan – was introduced in 1990 (Rigauts et al., 1990). This was followed by the introduction of multi-slice scanning in 1998, with a scanner capable of 4-slice acquisitions (Taguchi et al., 1998). Multi-slice scanning implicated the widening of the beam and adding several rows of detectors in the z-direction. This allowed the simultaneous acquisition of several slices of data while reducing the heat loading and the acquisition time (Goldman, 2008). More developments in the multi-slice CT have been observed, going from 16-slice acquisition in 2002 (Flohr et al., 2002) to 320-slice acquisition in 2007 (Rybicki et al., 2008). The increase of acquired slices augmented the z-axis field of view, enabling more coverage (Goldman, 2008).

In 4D-CT, a 3D-CT volume containing a moving structure is imaged over a period of time (Katsuyuki Taguchi, 2003). The images acquired are reconstructed retrospectively. This means that a separate signal is acquired simultaneously and synchronized with the image acquisition. In case of the breathing motion, the respiratory signal is used to sort the partial images into the correct breathing state and then are combined into a single volumetric 3D image of the breathing state (Vedam et al., 2003).

The use of 4D-CT for radiotherapy purposes is an advantage in treatment planning since it allows to create robust treatments by adding safety margins to the CTV, while reducing the chances of a geographic miss. During planning, by analyzing 4D-CT images, it is possible to reduce the PTV, since the intra-fraction movement is considered (Kwong et al., 2015).

The radiation dose to which the patient is exposed during a CT is affected by five parameters: current, kilovoltage, pitch (table speed), detector collimation and scan coverage. Using the latest generation CT scans, which have the property of a broad field of view, it is possible to use a reduced radiation dose technique due to the inherent natural contrast between soft tissue and the low density of the lungs (Kwong et al., 2015).

2.5.2 Cone beam computed tomography

As mentioned in the previous section “Dose distribution robustness”, IGRT allows to reduce uncertainties through the course of treatment (Court, 2014) and CBCT is a popular choice due to good image contrast and signal-to-noise ratio (Groh et al., 2002). CBCT results from tomographic reconstruction of a series of planar images, obtained as the gantry rotates around the patient. These images can be acquired using the linac megavoltage cone beam computed tomography or by adding a separate kilovoltage source (kV-CBCT) attached to the gantry. While the concept of MV-CBCT is attractive as the beam source is the same as the one used to deliver the treatment, the image quality for low-contrast soft-tissue structures is inferior when compared to high-contrast structures. A way to overcome the soft-tissue contrast issues is to integrate the kV-CBCT in the linac (Mc Parland, 2009).

With highly conformal treatment techniques, such as IMRT, there is a need for increased precision in the location of the target and OAR. As a result, these CBCT images acquired with the kV-CBCT

integrated in the linac allow to monitor intra and inter-fraction change and to make an adjustment of the treatment as required (Mc Parland, 2009; Srnivasan et al., 2014).

Another use of the CBCT images acquired during the treatment is for fractional dose re-calculations. However, the image quality of CBCT is still inferior to CT, which results in incorrect Hounsfield units (HUs). HU is a relative quantitative measurement of radio density used in the interpretation of CT images, using the attenuation coefficient of radiation within a tissue during CT reconstruction, to produce a grayscale image (DenOtter et al., 2021; Fotina et al., 2012; Stock et al., 2009).

To face the poorer image quality of CBCT when compared to CT, image registration can be used. In image registration, two or more images of the same region acquired at different times are combined, allowing to obtain complementary information from different imaging modalities (Mani et al., 2013). Non-rigid (or deformable) image registration tracks voxel-to-voxel changes from one CT image to another, correcting them by mapping between volume elements in a subsequent image. Deformable registration can be used as opposed to rigid registration – in this case, the CBCT images are registered to the planning-CT (Hwang et al., 2009). Rigid registration is, however, more prone to inaccuracies caused by rigidly registering a non-rigid tissue and may not account for inter-fraction changes caused by weight changes, changes in the positioning of the patient and soft-tissue displacements due to breathing (Brock, 2007).

Chapter 3

Materials and Methods

This chapter describes the methodology followed in the present project. As the patients included in this study present different characteristics, this chapter begins with a patient and treatment characteristics overview. Patient characteristics include information in terms of sex, age at the time of treatment, primary tumor type and if the patient received treatment under general anesthesia, which is practice for patients younger than 4 years old. Moreover, an overview of treatment characteristics is provided, including the treatment technique (if patients received only a primary dose or a boost dose), number of fractions and PD.

The robustness evaluation was performed in terms of target coverage and hot spots of the whole lung and lung metastases, but also in terms of dose delivered to the OARs. For the whole lung, the volume in which coverage was assessed was the ITV of both lungs, as this is a patient-specific margin, while the PTV is institution-specific. However, robustness of the metastases was assessed on the PTV, which is the result of an expansion of the ITV by 5 mm.

The OARs considered in this study were the heart, liver, spleen, thyroid, and mammary glands, based on literature (Bosarge et al., 2016; Kalapurakal, Zhang, et al., 2013) and a list of constraints provided by a radiation oncologist of the department.

3.1 Patient and treatment characteristics

After institutional review board approval (WAG/mb/500028), anonymized data from 21 patients (11 males, 10 females) that received whole lung irradiation at the Department of Radiotherapy of the University Medical Center Utrecht, between March 2016 and December 2020, were included in the present study: one rhabdoid tumor, one epithelioid sarcoma, one synovial sarcoma, eight Ewing sarcoma and 12 Wilms' tumor patients. The patient data included in the study comprises planning-CT, CBCTs, treatment plans and structure delineations. The average patient age at the time of treatment was 7 years old (range 1-18 years old) and the prescribed radiotherapy dose was delivered to the patients using a 10 MV VMAT technique, recurring to one up to three arcs. Due to the young age of 6 patients (<4 years old), the radiotherapy treatment was delivered under general anesthesia. A full overview of patients' characteristics is listed in Table 3.1.

Since dose distributions differ a lot from patients that received only a primary dose to patients that received primary and boost doses simultaneously, the results of the study were divided into two sections: patients without lung metastases (11 patients) and patients with lung metastases (10 patients). This allows a more organized analysis because most patients that received only a primary dose present similar dose distributions. Conversely, patients that received primary and boost doses present more inhomogeneous

Table 3.1: Patient characteristics, including sex, age at the time of treatment, type of primary tumor and if the patient received treatment under general anesthesia. *Abbreviations: WT = Wilms' tumor, ES = Ewing Sarcoma.*

Patient number	Sex	Age at the time of treatment	Primary tumor	General anesthesia
1	F	8	WT	No
2	M	1	Rhabdoid tumor	Yes
3	F	4	WT	No
4	F	2	WT	Yes
5	M	7	WT	No
6	F	2	WT	Yes
7	M	6	WT	No
8	M	6	WT	No
9	F	8	WT	No
10	F	3	WT	Yes
11	F	5	WT	No
12	M	9	WT	No
13	M	16	ES	No
14	M	4	ES	Yes
15	M	18	Epithelioid sarcoma	No
16	F	16	Synovial sarcoma	No
17	M	4	ES	No
18	M	13	ES	No
19	F	3	ES	Yes
20	M	12	ES	No
21	F	7	ES	No

dose distributions due to the high doses delivered to the metastases and so these dose distributions need a more detailed assessment. The patients without metastases received a fractional dose of 1.5 Gy, resulting in a total dose of 15 Gy throughout 10 fractions, except patient 2, who received a fractional dose of 1.8 Gy in 6 fractions. The patients with metastases were treated with the simultaneous integrated boost (SIB) technique, which delivers a primary dose to the whole lung and an integrated boost dose only to the metastases. These patients received a primary dose of either 12 or 15 Gy in a total of 8 or 10 fractions, depending on the patient, and boost doses ranging from 22 to 45 Gy. All the information from these patients is represented in Table 3.2.

Although the International Society of Paediatric Oncology (SIOP)-2001 protocol recommends a PTV margin of 10 mm around the CTV, at the Department of Radiotherapy of the UMCU, a 5 mm PTV is used around a patient-specific ITV, obtained by visual inspection of the difference phases of the 4D planning-CT. Due to large inter-fraction patient position variations, the PTV of one patient was later adapted to 8 mm.

The OARs considered in this study were the heart, spleen, liver, mammary glands and thyroid, due to their proximity to the lungs. However, not all these organs are delineated for all patients and so it is not possible to extract information about the dose being delivered to each organ for some patients.

3.2 4D-CT and CBCT imaging

For treatment preparation, patients were placed in an individualized vacuum mattress (Bluebag, Elekta, Stockholm, Sweden), except patient 1, in a supine position with the arms wide along the body or

Table 3.2: Treatment characteristics, including treatment technique, number of fractions and prescribed dose. *Abbreviations: SIB = Simultaneous Integrated Boost*

Patient	Technique	Number of fractions	Fractional dose (in Gy)		Total dose (in Gy)	
			Primary	Boost	Primary	Boost
1	SIB	8	1.5	2.75	12	22
2	No boost	6	1.8	-	10.8	-
3	SIB	8	1.5	2.75	12	22
4	SIB	8	1.5	2.75	12	22
5	No boost	10	1.5	-	15	-
6	SIB	8	1.5	2.75	12	22
7	No boost	10	1.5	-	15	-
8	SIB	8	1.5	2.75	12	22
9	No boost	10	1.5	-	15	-
10	SIB	10	1.5	2.8	15	28
11	SIB	8	1.5	2.75	12	22
12	SIB	8	1.5	2.75	12	22
13	No boost	10	1.5	-	15	-
14	SIB	10	1.5	3.5	15	35
15	No boost	10	1.5	-	15	-
16	No boost	10	1.5	-	15	-
17	No boost	10	1.5	-	15	-
18	No boost	10	1.5	-	15	-
19	No boost	10	1.5	-	15	-
20	SIB	10	1.5	4.5	15	45
21	No boost	10	1.5	-	15	-

above the head. A 4D-CT from the lungs until the lower abdomen was acquired for each patient in treatment position. The 4D-CT images were obtained as a series of 10 phases using a 16-. 40-, or 64-channel detector scanner (Brilliance, Philips Medical Systems, Best, The Netherlands) and scans with a slice thickness of 2 mm were acquired. The planning-CT was obtained by taking the pixel-by-pixel average of the 10 phases of the 4D-CT that range from 0 to 90%, in 10% intervals, covering a full breathing cycle. During treatment, daily CBCT images were acquired for every treatment fraction using the XVI 4.5.1 on-board CBCT imaging system (Elekta, Stockholm, Sweden).

During treatment, daily CBCT images were acquired for every treatment fraction using the XVI 4.5.1 on-board CBCT imaging system (Elekta, Stockholm, Sweden).

3.3 Robustness assessment against intra-fraction anatomical changes

The study of robustness for intra-fraction anatomical changes started by visual inspection of all ten phases of the 4D-CT and selection of the maximum expiration and inspiration phases, as seen in Figure 3.1, using Volumetool, an in-house built delineation software (Bol et al., 2009). The identification of such phases was performed mostly by inspection of the diaphragm position. For younger patients, the difference in terms of lung volume and diaphragm position between two consecutive phases was not always clear and, for these cases, a subtraction between the two phases in question was obtained to identify the one corresponding to the extreme breathing phase.

The contours used for the minimum and maximum phases were the same as the ones of the planning-

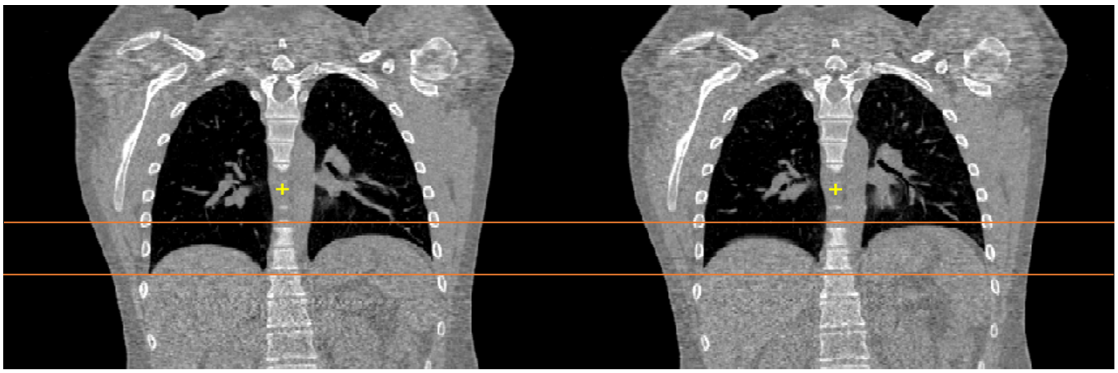

Figure 3.1: Difference between the maximum (left) and minimum (right) respiration phases for patient 14.

CT (clinical contours delineated by the radiation oncologist), changing only the body contour. This was done to account for the abdominal wall changes during the breathing cycle, due to the contraction and relaxation of the diaphragm. After creating the new body contour, a slice-by-slice verification had to be performed due to some delineation inconsistencies such as: inclusion of the treatment table as part of the body contour due to similar HUs; structures outside the body contour in the minimum phase, such as the liver, mammary glands, and lung PTV; interference in the body contour by the port-a-cath; influences in the body contour by a deformable rubber belt fixed to the patients' chest, used to obtain respiratory trace measurements for pulmonary gating.

The maximum expiration and inspiration phases were exported from Volumetool and imported into Monaco treatment planning system (Elekta, Stockholm, Sweden) and the treatment plan was recalculated using the same isocenter as per the original plan used clinically.

3.4 Robustness assessment against inter-fraction anatomical changes

The study of robustness for inter-fraction anatomical changes was performed by calculating the fractional doses in the CBCT images and accumulating the resulting doses. For this purpose, all CBCTs were labeled according to the fraction they corresponded to, from one to eight or ten, depending on the patient. Since the CBCT images are not calibrated, there is no correspondence between HUs and electron density (ED), thus the planning-CT was deformably registered to each CBCT using EVolution (Denis De Senneville et al., 2016) and outside the field of view of the CBCT, the information of the planning-CT was used. This algorithm was previously validated for CT-CBCT registrations for kidney and lung cancer patients (Zachiu et al., 2017). The performance of the registration was evaluated by visually inspection of all registered-CTs, patient by patient. Since the CBCTs were acquired with less imaging dose than a standard adult protocol, an accurate tracking of daily deformations cannot be guaranteed for all structures. For this reason, all delineations from the planning-CT were used in the registered-CTs, except for the body contour. This structure was re-delineated for the same reasons as the ones mentioned for the intra-fraction study.

The registered-CTs were imported in the treatment planning system and the plan was recalculated for each fraction, using the same isocenter as per the original plan. The new plans were then rigidly accumulated to obtain the accumulated dose and the dose-volume histogram (DVH) parameters were retrieved from Volumetool.

3.4.1 Dosimetric evaluation

3.4.1.1 Target coverage and hot spots

To assess lung ITV coverage without the influence of the boost doses, a new structure including the ITV of both lungs minus the PTV of metastases was created, since robustness of the dose distribution of the metastases was evaluated on the PTV. This allows a more truthful hot spot (volume of lung ITV receiving more than 107% of the PD) assessment of the primary dose distribution, as it excludes most of the high dose fall-off from the metastases. Considering the lung ITV and PTV of the metastases, the DVH parameters considered in this study for the evaluation of the robustness of the dose distributions were the mean dose (D_{mean}), percentage of lung ITV volume that received at least 95% of the PD ($V_{95\%}$) and percentage of lung ITV volume that received at least 107% of the PD ($V_{107\%}$). A plan was considered robust if, considering the ITV of both lungs and the PTV of the metastases, $V_{95\%} > 99\%$ and $V_{107\%} < 1\%$, although $V_{107\%} < 10\%$ was also acceptable (as long as the overdosage stayed within the lung PTV). Additionally, for the PTV of the metastases, $V_{95\%} > 95\%$ was also acceptable, as long as proper ITV coverage was verified. For these parameters, values obtained for the two considered respiratory phases that differed more than 5% from the original plan were considered clinically relevant.

3.4.1.2 OAR coverage and constraints

To evaluate the robustness of the dose to the OARs, the D_{mean} and near maximum dose ($D_{2\%}$) were considered. The differences between the recalculated and the original plans were considered clinically relevant if they were over 3 Gy. In terms of percentage of the PD, this means that a difference is considered clinically relevant if it is greater than 20% or 25% for a primary dose of 15 Gy or 12 Gy, respectively. The retrieved DVH parameters were then compared to a list of constraints provided by a radiation oncologist and these are: 5 Gy for the thyroid and mammary glands, 10 Gy for the spleen, 28 Gy for the liver and as low as reasonably achievable for the heart, but with mean dose values of approximately 6-8 Gy for PDs between 12-15 Gy.

Since the heart is a fairly large organ adjacent to both lungs, the $D_{2\%}$ of the heart was evaluated. Evaluating these parameters instead of the D_{mean} provides more accurate information in terms of local hot spots within this organ. Furthermore, for the patients with boost doses close to the heart that presented high values of $D_{2\%}$, the volume receiving at least 21.6 Gy ($V_{21.6Gy}$) was obtained. This is an important indicator in terms of heart sparing, since the volume receiving more than 21.6 Gy represents an increased risk of future heart failure.

Chapter 4

Results and Discussion

This chapter comprises the results obtained for the recalculation of photon treatment plans against intra and inter-fraction anatomical changes and consequent discussion.

In the following sections, patients are divided in patients with and without lung metastases. Patients without metastases received only a primary dose to the whole lung, while patients with metastases received a primary dose to the whole lung and an additional boost dose to the metastases.

4.1 Robustness of photon dose distributions against intra-fraction anatomical changes

The following section concerns the study of robustness of photon dose distributions against intra-fraction anatomical changes, which was performed by recalculating the original plan for the two extreme breathing phases.

4.1.1 Patients without lung metastases

4.1.1.1 ITV coverage and hot spots of the lungs

Mean $V_{95\%}$ was 99.8% ± 0.1% (range [99.3%; 100%]) for the original dose distribution and 99.% ± 0.1% (range [99.3%; 99.9%]) and 99.8% ± 0.1% (range [99.0%; 100%]) for the plans recalculated for the minimum and maximum lung expansion phases, respectively. So, lung ITV coverage was achieved for all patients for both phases. Conversely, mean $V_{107\%}$ of the lungs ITV was 0.5% ± 0.2% (range [0.0%; 1.6%]), 1.1% ± 0.3% (range [0.0%; 3.4%]) and 3.5% ± 0.9% (range [0.1%; 11%]) for the original, minimum lung expansion phase and maximum lung expansion phase dose distributions, respectively. As there are no differences greater than 5% between the recalculated and the original plans, average lung ITV coverage and hot spots indicate that the recalculated plans are robust against intra-fraction changes.

The $V_{95\%}$ and $V_{107\%}$ values per patient are represented in Figure 4.1. The observation of the results from the figure suggests that lung ITV coverage was indeed achieved for all the patients and all considered respiratory phases, but hot spot values were above the constraint when considering the maximum expansion phase of patients 13, 15, 17 and 18, the original and minimum expansion phases of patient 19, the minimum and maximum lung expansion phases for patients 5, 7 and 9, and all the phases for patient 16. A tendency for an increase of $V_{107\%}$ is noticeable when considering the maximum expansion phase (corresponding to the maximum inhalation phase of the breathing cycle). This increase is clinically relevant only for patients 5 and 16. The $V_{107\%}$ values of patient 5 increased from 0.2% in the original dose

distribution to 6.4% in the maximum expansion phase, while patient 16 went from 1.6% in the original dose distribution to 11.0% in the maximum lung expansion phase.

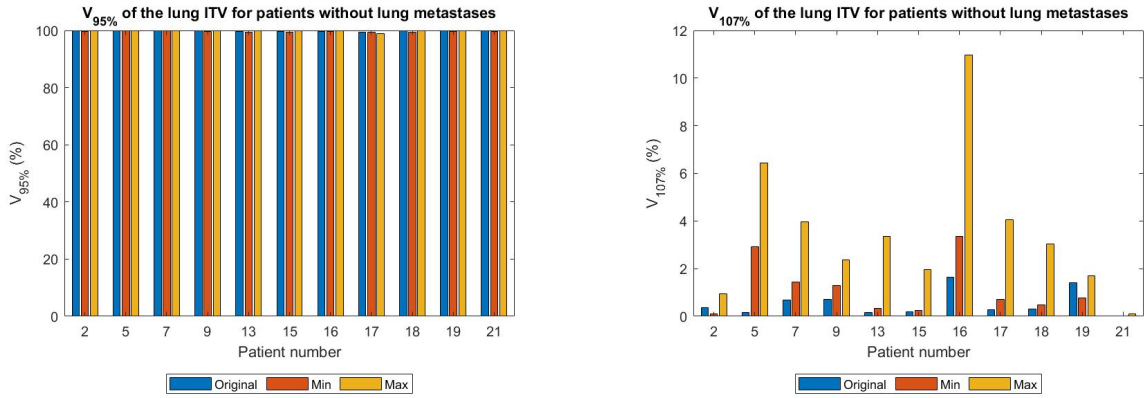

Figure 4.1: $V_{95\%}$ and $V_{107\%}$ values of the lung ITV for patients without lung metastases. The blue, orange, and yellow bars correspond to the original, minimum expansion and maximum expansion dose distributions, respectively.

The patients with clinically relevant differences were investigated. The increase in $V_{107\%}$ when considering the maximum lung expansion phase is related to a large displacement of the diaphragm towards the abdomen in a situation in which the patients were breathing very deeply, especially considering patient 16. By inspecting the dose distribution of this patient, in the original plan (Figure 4.2, top) there is part of the diaphragm inside the lung ITV, while in maximum lung expansion phase (4.2, bottom), there is lung tissue in the same location. Such displacement affects ED at the base of the lung ITV, since for the same position instead of finding part of the diaphragm there is lung tissue, with approximately three times less ED. Calculating the plan for a volume with a certain ED (in this case, muscle), there is a certain path length expected for the photons. The presence of lung tissue decreases the ED in that region, decreasing the path length and resulting in a hot spot.

The ITV margin is added to account for the breathing motion, being a patient-specific margin defined by inspection of all phases of the planning-CT. Although the hot spots presented for all the patients stay mostly within the lung PTV and there are no cases of underdose, there is still the need to account for the unpredictability of the respiratory movement. The amplitude of the breathing motion can greatly influence the ED in a specific region within the target volume and consequently influence the treatment outcome, even when the treatment is planned on an ITV margin. A study by Huijskens et al. investigated if children's diaphragm motion during radiotherapy could be accurately predicted by the planning 4D-CT acquired before treatment (Sophie C. Huijskens et al., 2018). The investigation was performed by analysing CBCT images acquired during treatment. Since some patients in Huijskens' study had more than one CBCT taken within one treatment session, a better assessment of the intra-fraction motion is possible, as different breathing cycles other than the one used to delineate the ITV margin are being investigated. Of the 12 patients included in the study, 7 presented significant shifts in terms of diaphragm position, suggesting that it is not possible to accurately predicted intra-fraction changes with the planning-CT only. However, Huijskens' study included an older patient cohort (range 8-17 years old) and excluded one patient that received treatment under general anesthesia. Therefore, the study can be compared with the example given in Figure 4.2, but not with the remaining patients included in this study.

Based on the results of Huijskens' work and a study by Panandiker et al. (Sophie C. Huijskens et al., 2018; Pai Panandiker et al., 2012), in which intra-fractional organ motion was assessed using 4D-CT

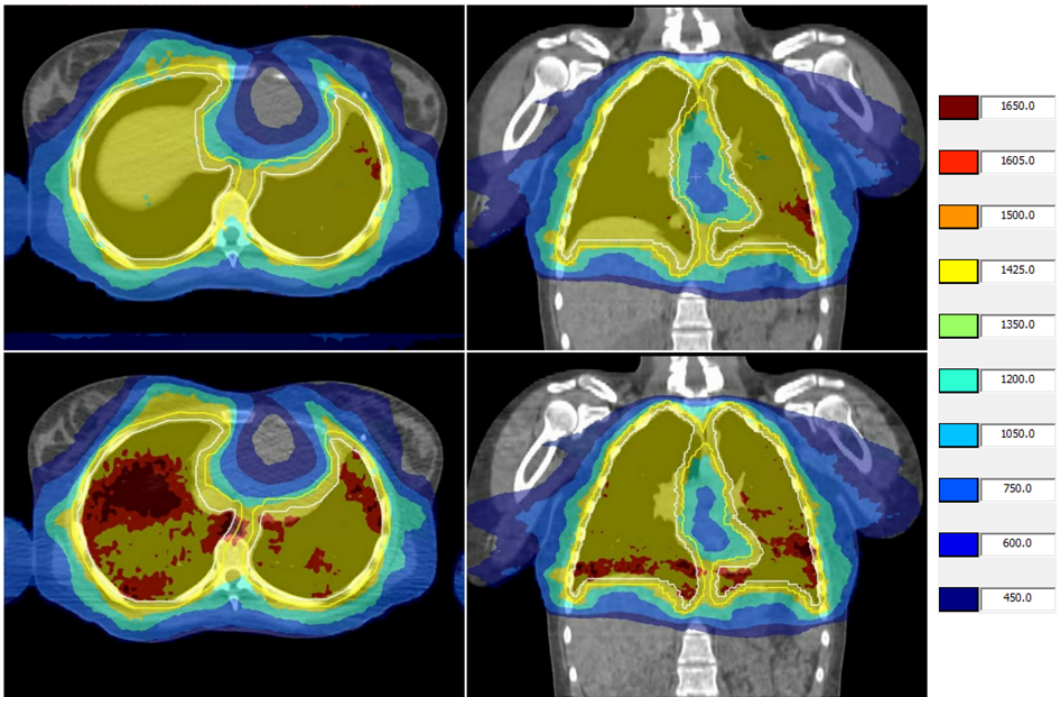

Figure 4.2: Dose distribution, in cGy, of patient 16 on the original (top) and maximum lung expansion phase (bottom) observed in the transverse (left) and coronal (right) planes, with the ITV (white) and PTV (yellow) contours.

and was found to be related to the patients' age, a relationship between age at the time of treatment and differences observed in terms of dose distribution was investigated. The patient presented in Figure 4.2, for example, corroborates the hypothesis that older patients present larger diaphragm displacements and consequently increased $V_{107\%}$ values. However, by inspecting the results of the remaining patients, it is possible to observe that there is no correlation between patient age and $V_{107\%}$ values — patients 5 and 21 were both 7 years old at the time of treatment and while patient 5 presents a clinically relevant difference between the original plan and the plan recalculated for the maximum lung expansion phase, patient 21 presents no hot spots within the lung ITV in all three phases. In Panandiker's study, patients were divided in two age groups, 2-8 years old and 9-18 years old and inferior mean respiratory diaphragm motion was associated with the younger age group. However, all patients from the younger patient group received treatment under general anesthesia, unlike in the present study (in which only patients younger than 4 years old did). Two other studies divided their patients into two age groups (patients younger and older than 9 years old), but found no clinically significant correlation between respiratory-induced diaphragm motion and age (Sophie C Huijskens et al., 2017; Guerreiro et al., 2018). Furthermore, the same studies reported that differences in amplitude of respiratory-induced diaphragm motion in patients treated with or without general anesthesia were found to be insignificant, which was also found to be true for this patient group.

Besides adding safety margins around the target volume during free breathing (which encompasses adding a large ITV margin to account for large diaphragm movements that might significantly change throughout the course of treatment), there are other techniques to account for respiratory motion. They include immobilizing the target volume during treatment delivery (by using a plate to physically compress the abdomen, which in turn results in smaller motion range), respiratory gating, and real-time tumor tracking. With the exception of real-time tumor tracking, all these techniques have the advantage of minimizing target motion during treatment. Less target motion allows the use of smaller ITV margins, which results in less dose being delivered to surrounding OARs. Furthermore, respiratory gating using deep

inspiration breath hold has been reported to be feasible in patients as young as 5 years old (Gorgisyan et al., 2017), without affecting treatment duration (Demoor-Goldschmidt et al., 2017). This treatment technique poses as a good option to deliver radiotherapy to children with large breathing movements in play, although further studies need to be completed.

4.1.1.2 Dose to the OARs

The average doses to the OARs as a percentage of the respective PD are present in Table 4.1. The $D_{2\%}$ values of the heart are around 100% of the PD, which is expected due to proximity of the heart to the lungs, with an overlap of heart and lungs ITV structure in some cases. Overall, mean OAR dose values are constant when comparing the plans recalculated on the extreme breathing phases with the original plan, with no clinically relevant differences to report.

Table 4.1: D_{mean} and $D_{2\%}$, in percentage, comparison between the extreme breathing phases and the original dose distributions of patients without lung metastases. The values are represented as a percentage of the respective PD. *Abbreviations: MG = mammary glands, SD = standard deviation.*

Structure	Parameter	Mean ± SD (%)			Range (%)		
		Original	Min	Max	Original	Min	Max
Heart	$D_{2\%}$	100.6 ± 0.4	100.4 ± 0.5	101.3 ± 0.5	[98.7; 103.1]	[98.2; 103.4]	[98.7; 104.5]
Liver	D_{mean}	46.6 ± 3.3	46.6 ± 3.3	47.1 ± 3.4	[27.4; 61.6]	[27.1; 61.3]	[27.2; 61.8]
Spleen	D_{mean}	54.0 ± 2.9	54.3 ±2.8	54.8 ± 2.8	[40.5; 69.9]	[41.8; 70.7]	[41.9; 71.7]
Left MG	D_{mean}	45.7 ± 7.6	45.6 ± 7.8	47.4 ± 8.2	[25.7; 80.8]	[25.9; 81.4]	[27.2; 86.9]
Right MG	D_{mean}	47.7 ± 8.9	47.1 ± 8.6	49.6 ± 9.7	[24.2; 89.5]	[24.3; 86.7]	[24.5; 97.3]
Thyroid	D_{mean}	14.5 ± 1.7	14.0 ± 1.6	14.0 ± 1.6	[6.3; 22.0]	[6.0; 20.9]	[6.1; 20.7]

Regarding the dose delivered to the OARs per patient, the values retrieved are in Figure 4.3. The dose constraints are represented in the figure as horizontal lines. The $D_{2\%}$ in the heart is above the constraint for most patients, as well as the mean dose in the mammary glands. The differences in the considered dosimetric parameters between the original dose distribution and the ones computed on the two extreme breathing phases are smaller than 3 Gy, thus the original dose distribution can be considered robust.

Regarding the administered dose to the OARs, the liver, spleen and thyroid were the organs expected to more easily meet the desired dose constraints. This is proven by the fact that only one patient in this study, patient 16, presented dose to the spleen above the 10 Gy constraint, which is explained by the large differences in breathing amplitude observed in Figure 4.2. The below-constraint doses of the liver and spleen are due to the fact that, although the delineations of these organs overlap with lung ITV and PTV, these are fairly large organs compared to the other OARs like the mammary glands and thyroid. This means that, even if some differences are observed in the upper part of the liver or spleen (the part that would be more influenced by the diaphragm motion and consequently would result in different dose distributions in the lung), the bottom part is receiving virtually no dose. This can be observed in the example provided by Figure 4.4. This assumption is supported by studies of intra-fraction organ motion of abdominal organs in pediatric patients, with reports of average liver and spleen displacements in the cranio-caudal direction to be smaller than 3.5 mm (Kannan et al., 2017; Uh et al., 2017; Guerreiro et al., 2018). Moreover, there is less breathing motion in the apex of the lungs as compared to the diaphragm and the thyroid is not an adjacent organ to the lungs like the spleen and liver are. These factors culminate in the low dose values observed for the thyroid. Regarding the heart and mammary glands, there is a considerable number of patients receiving doses above the defined constraint. This is an expected outcome of the treatment, as these are the OARs closest to the target volume and more affected by the dose fall-off from the primary lung dose.

4. RESULTS AND DISCUSSION

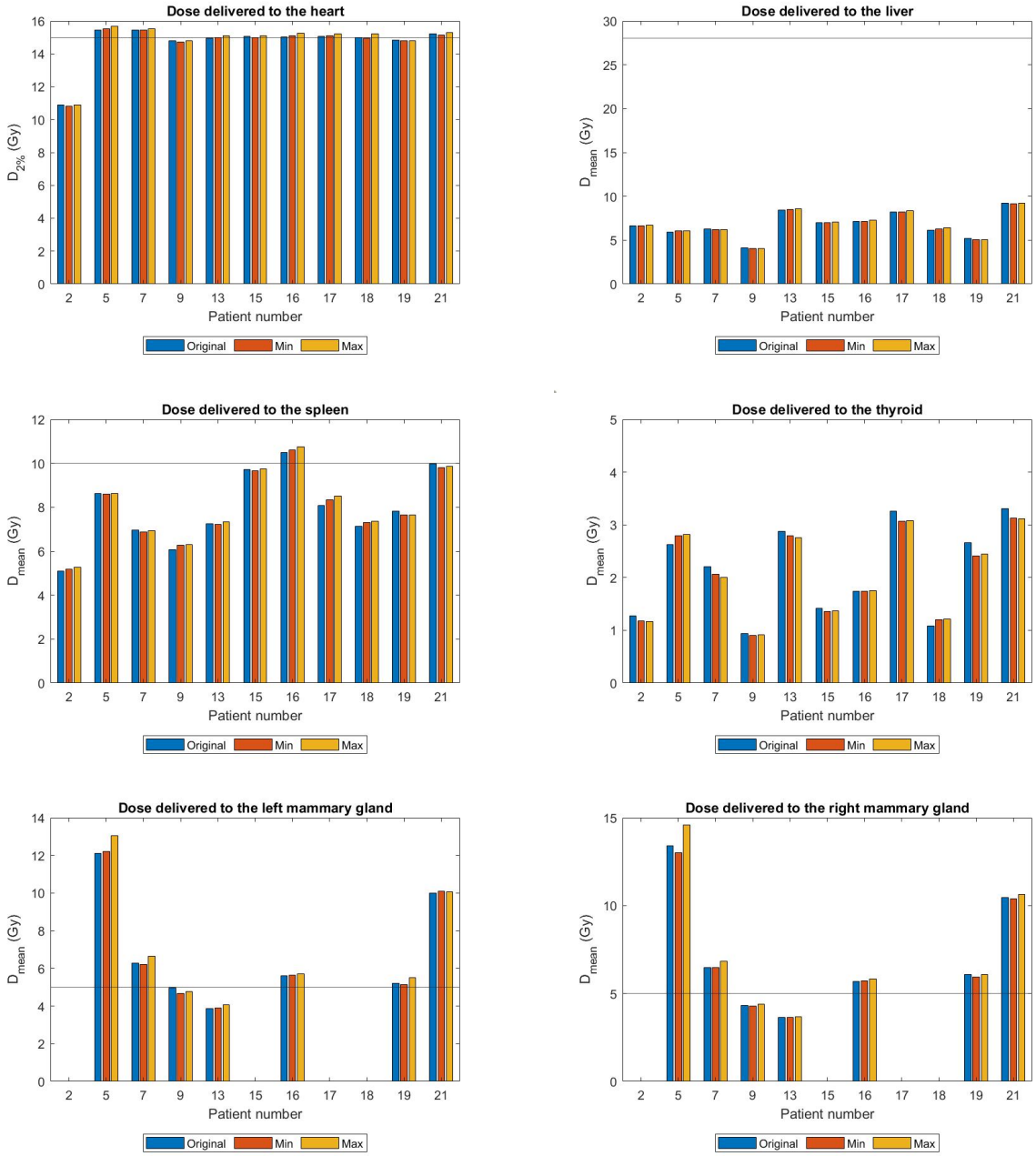

Figure 4.3: OAR dose values obtained for patients without lung metastases. The blue, orange, and yellow bars correspond to the original, minimum expansion and maximum expansion dose distributions, respectively, and the horizontal lines correspond to the dose constraint per organ.

The heart is the most important OAR to spare when delivering WLI and irradiation of the heart can cause severe complications. This becomes of special importance since each part of the heart has its own function that cannot be compensated by another (Tezcanli et al., 2011). Studies have associated heart irradiation to several disorders affecting the endocardium, myocardium, pericardium, coronary arteries, conduction system and cardiac valves. The Institute Gustave Roussy report indicated that the 20-year incidence of congestive heart failure was 18% after a mean cardiac dose greater than 6.7 Gy, and the Childhood Cancer Survival Study showed that cardiovascular disease and secondary malignancies were the main causes of morbidity and mortality in long-term survivors (Pein et al., 2004; Daniel A. Mulrooney et al., 2020). Moreover, studies have reported a cardiac dose above 15 Gy to be associated

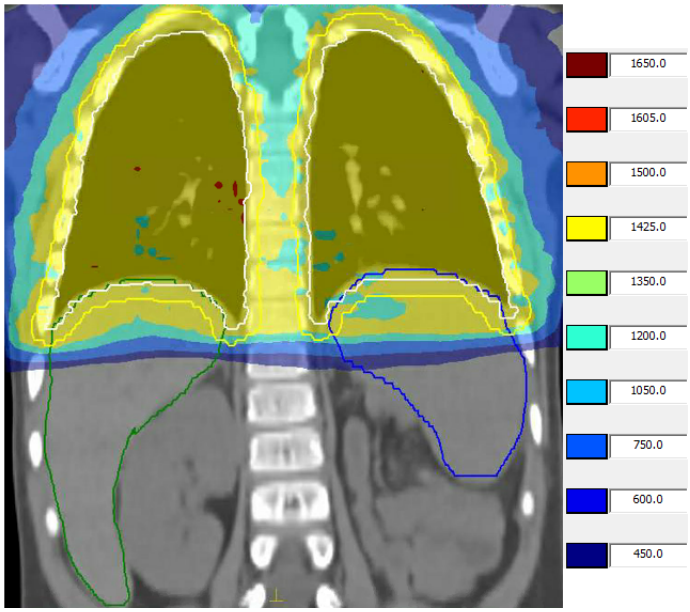

Figure 4.4: Position of the spleen (blue) and liver (green) in relation to the lung ITV (white) and PTV (yellow) delineations considering the primary dose being delivered to patient 10, with the respective dose distribution.

with cardiomyopathy and valvular disease (Daniel A Mulrooney et al., 2016). As children are more susceptible to radiation-induced cancers, researchers have attempted to improve treatment techniques in order to avoid irradiation of surrounding healthy tissue. This was accomplished by Bosarge et al., who demonstrated the advantages of inverse-planned AP/PA (IP-AP/PA) and VMAT over the S-AP/PA technique in terms of OAR sparing, and also by Kalapurakal et al. and their cardiac-sparing IMRT technique (Bosarge et al., 2016; Kalapurakal, Zhang, et al., 2013). However, target coverage is of priority in treatment planning, so when sparing the heart compromises target coverage, irradiating the heart becomes unavoidable. The treatment techniques previously described to decrease $V_{107\%}$ values within the lung ITV, mainly respiratory gating and breath hold, could also be employed to reduce heart dose, since smaller margins would be applied.

Another important OAR particularly challenging to spare are the mammary glands, as an attempt to keep the dose values in this organ within the constraint can lead to underdose on the anterior part of the lungs. Due to the differences in patient diameter observed during the selection of the extreme breathing phases, which even led to the need for a new body contour, clinically significant differences were expected to be observed between the recalculated and the original plans. Although above the constraint, the mean doses were robust against intra-fraction changes, with no differences larger than 3 Gy in the recalculated plans. It is important to discuss the definition of clinically relevant for OAR dose differences observed on the recalculated plans, as there are no guidelines to establish what is an acceptable difference. Thus, the 3 Gy threshold was defined for this specific study. Considering the mammary glands, this organ differs a lot in size between patients. This means that, for younger patients, this structure is smaller and, therefore, more sensitive to differences in ED or positioning variations in relation to larger structures. Additionally, the mean dose constraint for this OAR is quite low when compared, for example, with the liver. For this reason, the 3 Gy threshold might not be adequate, as the organ is expected to receive less dose. In the literature, Nyeng et al. considered a 1 Gy deviation in mean dose acceptable on their study of the dosimetric effect of inter-fraction anatomical changes during radiotherapy of esophageal cancer (Nyeng et al., 2015). Similarly, in a study of the dosimetric implications of inter-fraction changes in OARs during dose escalation for locally advanced lung cancer, the authors

considered a 1 Gy increase in mean lung dose and mean heart dose as an overdosage (Hoffmann et al., 2018). However, these studies were conducted with adult patients and not children. For future studies, it might be more advantageous to define a robustness evaluation dose value based on the constraint for that OAR, or consider the 1 Gy threshold as the clinically acceptable difference, as reported in the literature.

The use of proton beams has been demonstrated to be well tolerated by children with malignant tumors, ensuring good tumor control probability, prolonged survival and reduced risk of secondary malignancies (Paganetti et al., 2002; Cunningham et al., 2020). Moreover, proton therapy has been described in literature to be a feasible option to deliver whole lung irradiation to pediatric patients (Cunningham et al., 2020; Flampouri et al., 2021; Sha et al., 2021; Wong et al., 2021). Although no significant differences were observed in terms of target coverage, IMPT has shown to reduce mean dose to surrounding OARs, mainly heart and breasts, as compared to photon therapy techniques like IMRT and VMAT (Flampouri et al., 2021; Wong et al., 2021). However, proton therapy is a challenging technique, being more susceptible to uncertainties. First, the range uncertainty might alter the proton range and consequent dose distribution, resulting in a possible underdosage of the target or overdosage of OARs. Additionally, setup errors and intra-fraction anatomical changes, mainly the respiratory motion, can originate displacements of the tumor and surrounding tissues. Such displacements can change proton range and influence the dose distribution. This becomes especially relevant as the lung presents approximately one third of the density of, for example, the heart or the diaphragm. While Wong's study only considered children with target motion of less than 5 mm (as it has been reported in the literauture interplay effect for tumor motion inferior to 5 mm (Tsunashima, 2012; Boria et al., 2019)) eligible for treatment with IMPT, Cunningham et al. delivered proton therapy complemented with respiratory gating or breath hold techniques to patients that presented a diaphragmatic motion greater than 1 cm. Thus, proton therapy has been demonstrated to be a feasible technique and well tolerated, although it requires further investigation in terms of long term outcomes (Cunningham et al., 2020).

4.1.2 Patients with lung metastases

4.1.2.1 ITV coverage and hot spots of the lungs

Average lung ITV coverage of patients with lung metastases was 96.3% ± 3.5% (range [64.9%; 100%]) for the original plan, 96.0% ± 3.4% (range [65.2%; 100%]) for the minimum lung expansion phase and 96.9% ± 3.1% (range [69.2%; 100%]) for the maximum lung expansion phase. The desired average coverage ($V_{95\%}$ >99%) was not achieved due to the presence of an outlier, patient 14, whose coverage represents the minimum value in the range interval.

For the original plan, the average $V_{107\%}$ was 33.1% ± 9.1% (range [7.1%; 89.5%]), while for the minimum lung expansion phase it was 34.2% ± 9.1% (range [7.4%; 87.3%]) and for the maximum lung expansion phase it was 38.0% ± 9.2% (range [9.3%; 89.9%]).

The results of $V_{95\%}$ and $V_{107\%}$ per patient are presented in Figure 4.5, in which it is observed that only the target volume of patient 14 did not meet the desired coverage. When planning a treatment using the SIB technique, the radiation therapist first plans the dose for the metastases and afterwards adds the primary dose to the whole lung volume. In the case of patient 14, to avoid overdosing the metastases, lung ITV coverage had to be compromised in the original treatment plan.

The high values of $V_{107\%}$ present in the ITV volume are a consequence of the dose fall-off of the metastases, as it can be observed in the example on Figure 4.6. The $V_{107\%}$ values vary a lot between patients, which can be explained by the differences between prescribed boost doses, as it is the case for patient 20, with a 30 Gy difference between the primary dose to the lung (15 Gy) and boost dose to the

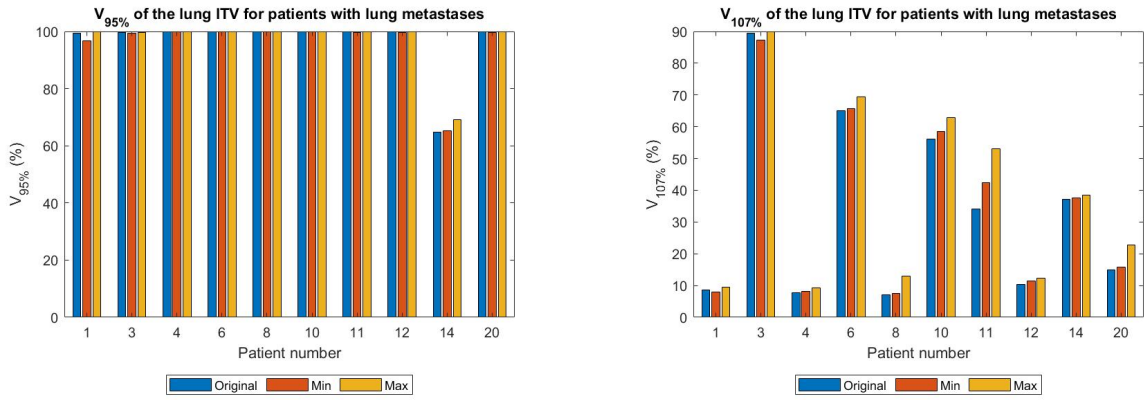

Figure 4.5: $V_{95\%}$ and $V_{107\%}$ values of the lung ITV for patients with lung metastases. The blue, orange, and yellow bars correspond to the original, minimum expansion and maximum expansion dose distributions, respectively.

metastases (45 Gy). This difference makes it difficult to achieve a dose fall-off steep enough to spare the lung immediately outside the metastases PTV, since an attempt at a steeper dose fall-off might result in an underdosage of the metastases.

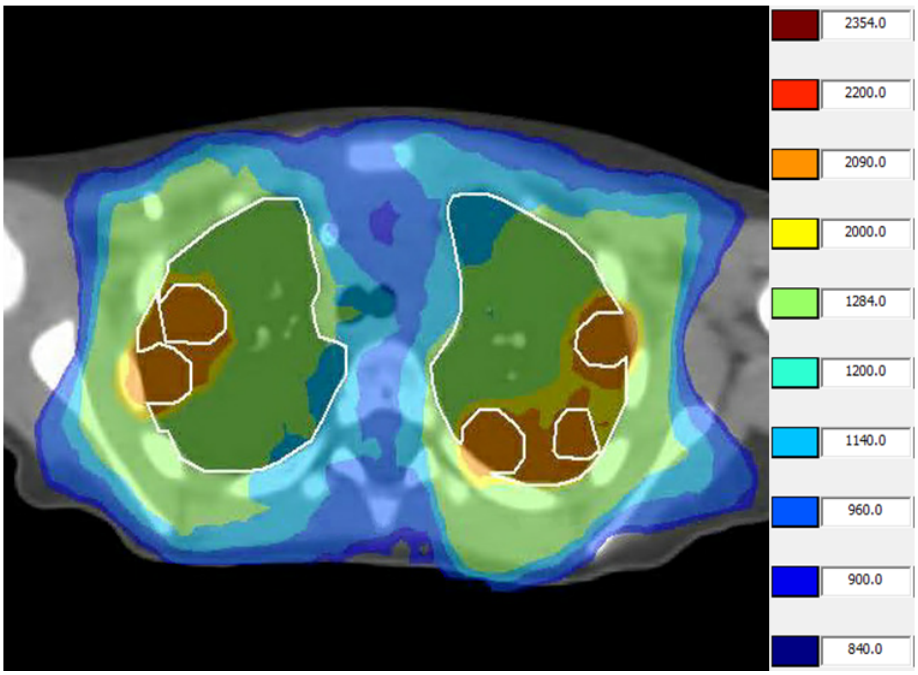

Figure 4.6: Example of dose fall-off outside the PTV of the metastases of patient 6, with the structure including the ITV of both lungs minus the PTV of metastases. Considering the dose levels, the $V_{107\%}$ corresponds to 1284 cGy (in green), which in this transversal plane mostly consists of the lung ITV volume.

Patient 11 presents a clinically relevant increase in $V_{107\%}$ in the maximum lung expansion phase, thus the original and maximum lungs expansion phase dose distributions were compared. From Figure 4.7 it is noticeable that there is more volume of the left lung receiving 107% of the PD during the maximum expansion phase (Figure 4.7, bottom). To understand the reason for such a difference, the ED within the ITV of the left lung was investigated. Mean ED was found to be 0.509 versus 0.422 in the averaged-CT and extreme breathing phase, respectively. Similarly to what was observed on the diaphragm region, a decrease in ED alters the path length of the beam, resulting in a larger hot spot.

Other factors that influence the $V_{107\%}$ values of lung ITV are the number and location of metastases

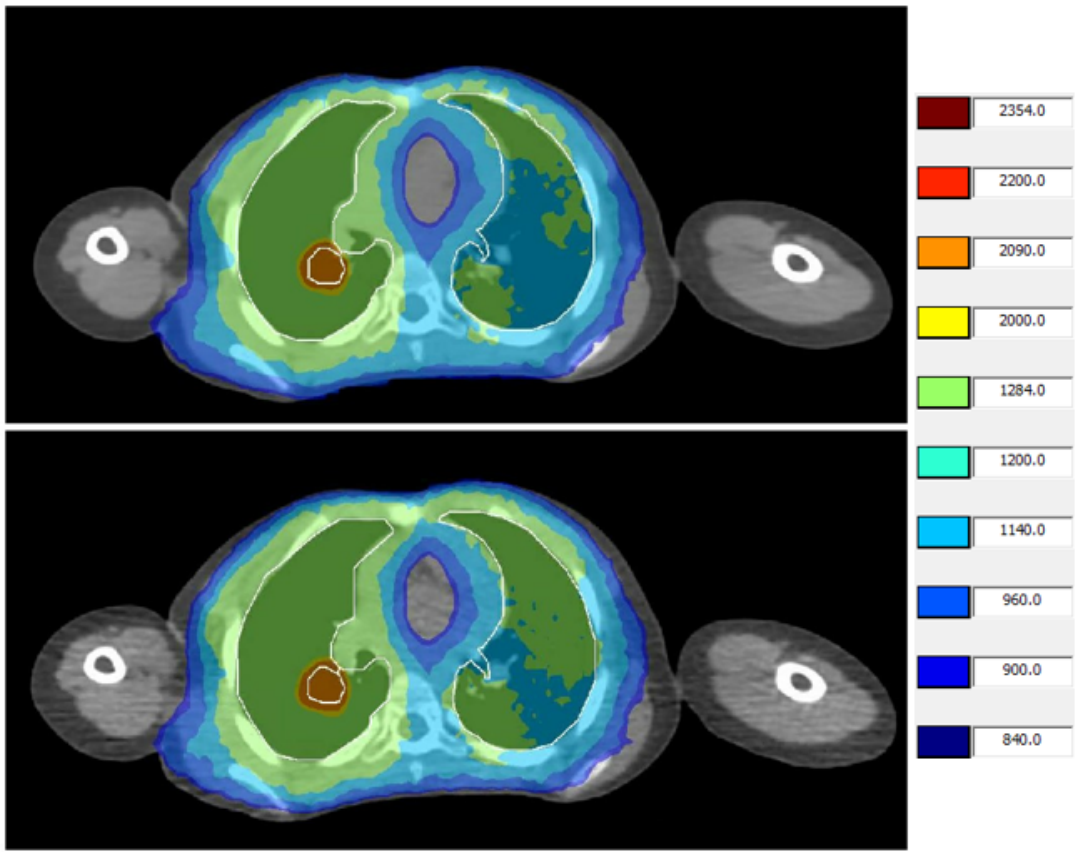

Figure 4.7: Dose distribution of patient 11 for the original plan (top) and for the plan recalculated on the maximum lung expansion phase (bottom). The white delineation corresponds to the structure comprising the lung ITV minus the PTV of metastases.

present in the lung. This applies to patients with more than three metastases, such as patients 3 (besides the two metastases in the lung the patient presents two metastases around the vertebrae, which also receive 22 Gy, resulting in a total of four metastases with overlapping dose fall-offs), 6, 10 and 14. The location of metastases in relation to certain OARs require a dose fall-off away from OARs, such as the heart and vertebrae, which will lead to higher doses in the rest of the lung. This is the result of a compromise, since these structures are being spared but there is significantly more lung volume receiving dose values greater than the primary dose. This is the case for patient 11, with two metastases in the posterior part of the lung near the heart and vertebrae.

With the exception of patients 1, 4, 8 and 12 (with hot spot volumes around 10%), $V_{107\%}$ values are of concern, as a large volume of lung without metastases is receiving more radiation than the primary dose. To better assess the primary dose being delivered to the lung ITV, the PTV of metastases was subtracted from this volume, creating a new structure. This new structure was created in an attempt to evaluate how the boost doses delivered to the metastases influence $V_{107\%}$ values on rest of the lung. The results were in line with the expected, as a photon treatment plan presents build up and exit doses, even with the employment of more conformal treatment techniques, such as VMAT. For this reason, in order to minimize irradiation of surrounding tissues, proton therapy can be an alternative to treat lung metastases. The use of proton therapy to deliver WLI to pediatric patients has been discussed in section 4.1.1. of this document, with significantly less mean OAR dose reported, while maintaining target coverage (Cunningham et al., 2020; Flampouri et al., 2021; Sha et al., 2021; Wong et al., 2021). However, these studies were conducted only with WLI patients receiving a primary dose to both lungs,

with no reports about the delivery of primary and boost doses simultaneously using proton therapy.

4.1.2.2 PTV coverage and hot spots of metastases

Average $V_{95\%}$ values were: 97.8% ± 0.7% (range [79.6%; 100%]) for the original plan, 99.1% ± 0.4% (range [88.1%; 100%]) for the minimum lung expansion phase and 97.1% ± 0.7% (range [84.8%; 100%]) for the maximum lung expansion phase. The required average PTV was not met for the original and maximum lung expansion plans, with very low coverage verified especially for metastasis 2 of patient 14, as it will be analyzed in more detail below. Average $V_{107\%}$ values, these were: 0.1% ± 0.1% (range [0.0%; 1.7%]) for the original plan, and 1.1% ± 0.7% (range [0.0%; 16.3%]) and 0.0% ± 0.0% (range [0.0%; 0.5%]) for the plans recalculated on the minimum and maximum lung expansion phases, respectively.

Table 4.2 presents the number of metastases per patient, as well as PTV coverage and hot spots. There are some large differences between the recalculated and the original plans, leading to the conclusion that PTV coverage is not robust against intra-fraction anatomical changes. Additionally, there are some cases of underdosage of the PTV, with $V_{95\%}$ <99%. However, since the PTV margin is added around the ITV to account for set up uncertainties, PTV coverage can be compromised as long as ITV coverage is achieved. In these cases, it is accepted for the PTV $V_{95\%}$ <95%. The ITV coverage of metastases was investigated per patient, concluding that all patients presented $V_{95\%}$ =100%.

For the considered clinically relevant $V_{95\%}$ and $V_{107\%}$ values — more precisely metastasis 2 of patient 1, metastases 2L and 5R of patient 6, metastasis 1 of patient 10 and metastases 2 and 4 of patient 14 — a more detailed investigation was performed. This was done by analyzing structure size and location within the lung and ED. Considering structure size, all PTVs were of small dimensions (<1 cm^3), which makes these structures more sensitive to anatomical changes caused not only by changes in scatter radiation due to the proximity to OARs, but also by changes in ED within the metastases. The underdosage of metastases was found to be associated with a decrease in ED within the PTV, resulting in less scatter photons and therefore less build up dose (as it is the case for metastasis 2 of patient 1 and metastasis 5R of patient 6). Conversely, the overdosage of metastases was observed to be associated with an increase in ED, which results in more scatter photons in the volume. This is the cause of the differences observed for metastasis 2L of patient 6, metastasis 1 of patient 10 (given as an example in Figure 4.8) and metastases 2 and 4 of patient 14.

Since small metastases are very sensitive to anatomical changes due to the respiratory motion, treatment delivery during free breathing is prone to induce underdoses or hot spots. Therefore, delivery under the breath hold technique, as previously suggested to reduce $V_{107\%}$ to the lung ITV, might be advantageous for this patient group. Resorting to the breath hold technique could minimize the effect of ED changes surrounding the metastases and consequently minimize the differences in scatter radiation observed in the extreme breathing phases.

Although no correlation was found between age at the time of treatment and the amplitude of respiratory-induced diaphragm motion (and consequent dose distribution recalculated in the extreme breathing phases), the relationship between these patients' characteristics and the cases of under and overdosage were investigated. The patients with clinically-relevant differences were patients 1, 6, 10 and 14, who at the time of treatment were 8, 2, 3 and 4 years old, respectively. This implies that, while patients 6, 10 and 14 received treatment under general anesthesia, patient 1 did not. Thus, no correlation can be established between patient age at the time of treatment and influence of the breathing motion on the dose distribution of metastases.

Table 4.2: Metastases PTV coverage and hot spots in the original plan and recalculated in the minimum (Min) and maximum (Max) lung expansion phases.

Patient	Boost	$V_{95\%}$ (%)			$V_{107\%}$ (%)		
		Original	Min	Max	Original	Min	Max
1	1	99.6	99.8	99.3	0	0	0
	2	99.8	99.7	85.4	0	0	0
3	1	98.0	98.9	95.3	0	0	0
	2	100	100	94.4	0	0	0
4	1	98.2	99.9	98.8	0	0	0
6	1L	99.7	100	100	0	0	0
	2L	90.8	98.6	92.6	0	0	0
	3L	100	99.5	98.8	0	1.3	0
	4L	99.1	99.1	99	0	0	0
	5L	98.2	98	97.7	0	0	0
	6L	99.7	100	98.1	0	0.3	0
	1R	99.6	100	97.5	0	0	0
	2R	94.6	98.7	98.5	0	0	0
	3R	95.2	99	95.4	0	0	0
	4R	99.1	100	98.7	0	0	0
	5R	98.8	98.3	92.2	0	0	0
	6R	100	100	99.4	0	1.3	0
	7R	100	100	97.4	0	0	0
8	1	99.0	99.8	99.8	0	0	0
10	1	99.8	100	99.7	1.7	13.8	0.5
	2	99.0	99.9	99	0	1.9	0.4
	3	98.6	100	100	0	0	0.5
11	1	99.7	100	100	0	0	0
	2	99.6	99.8	99.6	0	0	0
12	1	98.0	99.2	98.5	0	0.1	0
14	1	96.5	98	94.1	0	0	0
	2	79.6	88.1	84.8	0	0	0
	3	97.1	100	98.9	0	0	0
	4	95.7	99.1	98.4	0	16.3	0
	5	100	99.3	98.7	0	0.3	0
20	1	99.3	99.8	99.7	0	0	0

4.1.2.3 Dose to the OARs

The average dose to the OARs is represented in Table 4.3. There are no clinically relevant differences between the original plan and the plans recalculated in the extreme breathing phases.

The dose to the OARs per patient is represented in Figure 4.9. It is noticeable that the mean dose values in the mammary glands are above the constraint for a few patients and that these differ from left to right. This is due to the fact that the presence of boost doses leads to very different dose gradients for this group of patients, as opposed to a uniform dose distribution such as the one presented by the patients without metastases. Although the mean dose is above the constraint for these organs, the dose distributions are robust against the breathing motion.

Regarding the $D_{2\%}$ of the heart for the patients whose value is around 20 Gy, the $V_{21.6Gy}$ was evaluated. This value was provided by the radiation oncologist as an indicator for future heart failure. For

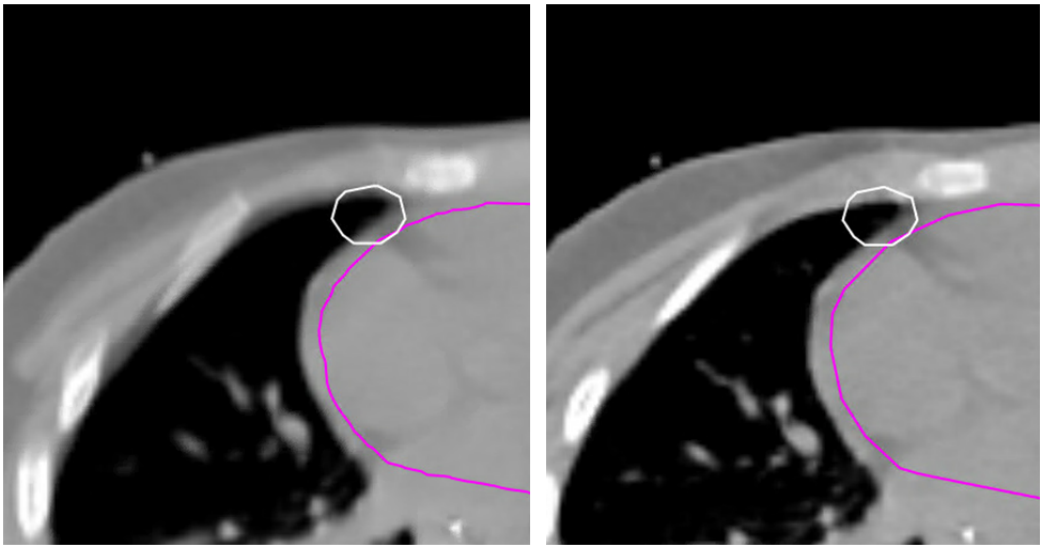

Figure 4.8: Position of the PTV of metastasis 1 of patient 10 (white) in relation to the heart (pink) in the averaged CT (left) and minimum lung expansion phase (right), one can observe the ED differences that result in the overdosage on the minimum phase are present. From the left to the right images there is a decrease of the volume of lung tissue within the PTV, resulting in an increase of ED and a consequent hot spot.

Table 4.3: D_{mean} and $D_{2\%}$, in percentage, comparison between the extreme breathing phases and the original dose distributions of patients with lung metastases. The values are represented as a percentage of the respective PD. *Abbreviations: MG = mammary glands, SD = standard deviation.*

Structure	Parameter	Mean ± SD (%)			Range (%)		
		Original	Min	Max	Original	Min	Max
Heart	$D_{2\%}$	116.6 ± 5.5	117.6 ± 5.2	118.0 ± 5.2	[98.8; 136.1]	[99.1; 134.7]	[99.4; 135.9]
Liver	D_{mean}	51.9 ± 9.1	51.8 ± 9.2	50.9 ± 9.2	[26.3; 98.6]	26.4; 98.1]	[26.4; 96.8]
Spleen	D_{mean}	49.8 ± 5.2	50.4 ± 5.2	50.5 ± 5.1	[28.3; 87.9]	[29.9; 87.8]	[29.8; 86.5]
Left MG	D_{mean}	50.3 ± 4.7	50.9 ± 4.8	52.9 ± 5.1	[25.7; 77.2]	[26.4; 79.6]	[26.4; 83.2]
Right MG	D_{mean}	50.7 ± 5.2	51.6 ± 5.2	52.9 ± 5.5	[31.6; 78.2]	[32.9; 79.3]	[31.8; 83.2]
Thyroid	D_{mean}	20.9 ± 2.4	20.7 ± 2.2	20.6 ± 2.2	[7.6; 33.8]	[8.1; 31.0]	[8.1; 29.9]

patient 10, $V_{21.6Gy}$ was 0.9% for the original plan, as well as for the plans recalculated on the extreme breathing phases. For patient 14, the $V_{21.6Gy}$ values were higher, with $V_{21.6Gy}$ reaching 1.6% for the original plan and 1.5% for both plans recalculated on the extreme breathing phases. To investigate the reason why the heart receives such a high dose for this patient, the dose distribution was analyzed (see Figure 4.10). It is possible to observe that there is a metastasis very close to the heart and that the PTV of the lesion and heart contours (in blue and pink in the figure, respectively) overlap, leading the radiation therapist to attempt to keep the fall-off dose away from the heart. This can be observed in Figure 4.10 by the asymmetrical dose gradient around the metastasis PTV, in which there is a steeper dose fall-off on the right side of the structure (the side on which the PTV and heart contours overlap), when compared to the dose fall-off observed on the left side.

The dose distribution presented in Figure 4.10 is an example of the unavoidability of the low dose bath to surrounding tissues characteristic of photon radiation. For metastases close to important structures, such as the heart, the use of proton therapy can prove advantageous, with less irradiation on surrounding OARs due to the finite range of protons. However, as proton beams are more sensitive to changes in density, there is a risk of dose misplacements. To face this uncertainty, the breath hold technique was studied for IMPT treatments of locally advanced non-small cell lung cancer (Gorgisyan et al., 2017). The results of the study demonstrated that the breath-hold approach is robust for IMPT,

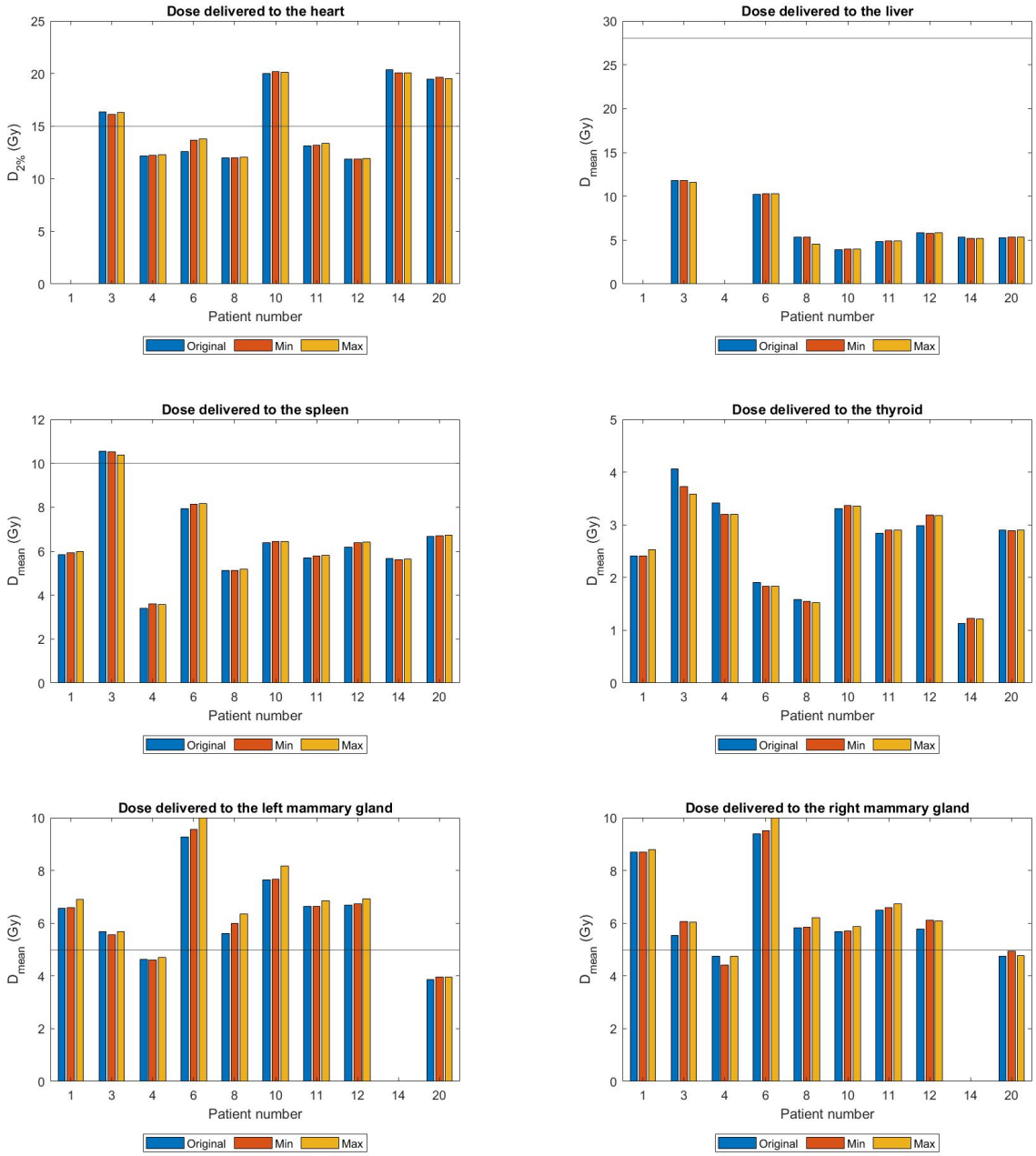

Figure 4.9: OAR dose values obtained for patients with lung metastases. The blue, orange, and yellow bars correspond to the original, minimum expansion and maximum expansion dose distributions, respectively, and the horizontal lines correspond to the dose constraint of each organ.

and treatment delivery was proven to be clinically feasible for most patients included in the study. However, the study was performed with an adult patient cohort. As children are more sensitive to radiation, combining the higher risk for late toxicity arising from the treatment with the size of lung metastases and heterogeinity of lung tissue, a geometrical miss when delivering a proton boost dose can have more severe consequences (Paulino et al., 2000; Yahalom et al., 2015).

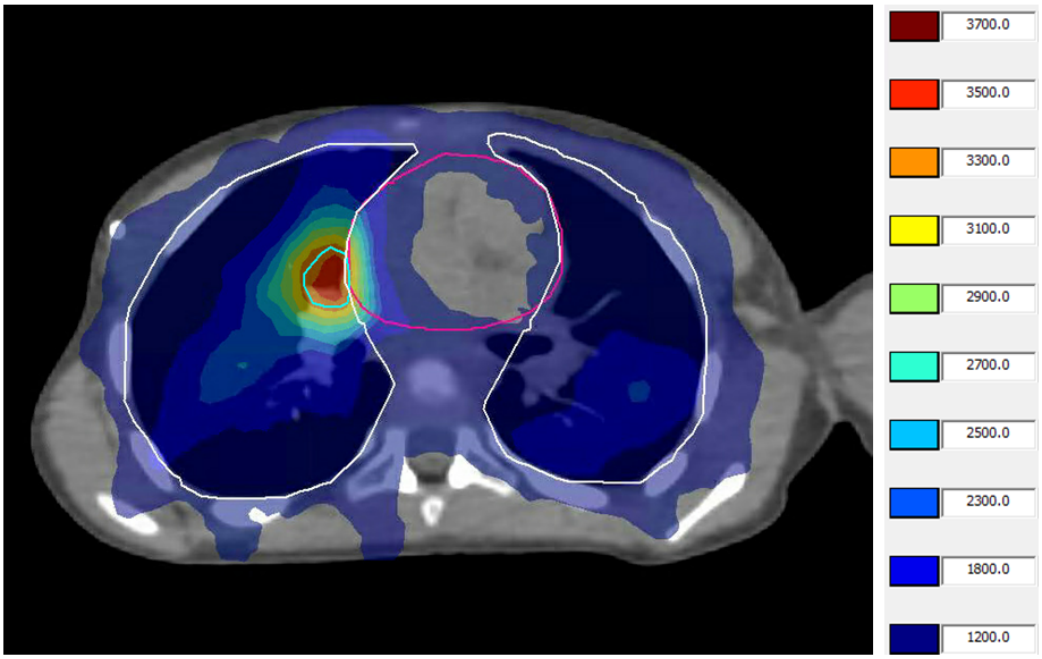

Figure 4.10: Position of the PTV of a metastasis (in blue) and the heart (in pink) in the transversal plane of patient 14, with the respective dose distributions (in cGy).

4.2 Robustness of photon dose distributions against inter-fraction anatomical changes

The second part of the results concerns the study of robustness of photon dose distributions against inter-fraction changes, which was performed by calculating the fractional doses on the CBCT images and accumulating the resulting doses.

4.2.1 Patients without lung metastases

4.2.1.1 ITV coverage and hot spots of the lungs

The average ITV coverage was 99.7% ± 0.1% (range [98.9%; 100%]) for the original dose distribution and 99.8% ± 0.1% (range [99.3%; 100%]) for the accumulated dose distributions. $V_{107\%}$ was 0.4% ± 0.1% (range [0.0%; 1.1%]) and 2.0% ± 0.6% (range [0.0%; 4.9%]) for the original and accumulated dose distributions, respectively. In general, ITV coverage was achieved and $V_{107\%}$ remained under the constraint.

The results per patient can be observed in Figure 4.11. The ITV coverage was achieved with no differences between the original and accumulated dose distributions. There is a tendency for an increase in $V_{107\%}$ when considering the accumulated dose distribution, with no clinically relevant differences to report, unlike what was observed on the intra-fraction study — the two patients that presented clinically relevant differences, patients 5 and 16, present dose differences within the defined threshold. Additionally, the higher $V_{107\%}$ values were approximately half than those of the intra-fraction study. This is in line with the results of a study by Huijskens et al., in which it was shown that intra-fraction anatomical changes, namely the breathing motion, are more irregular than the average respiratory motion throughout all fractions (Sophie C. Huijskens et al., 2018).

When calculating the fractional dose on the daily CBCTs, which were deformably registered to match the planning-CT, small inter-fraction differences were observed. These differences included mainly po-

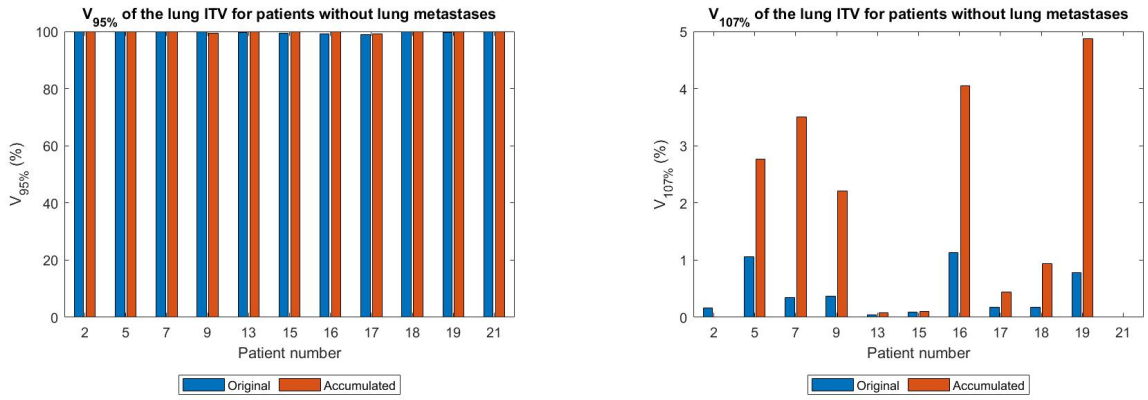

Figure 4.11: $V_{95\%}$ and $V_{107\%}$ values of the lung ITV for patients without lung metastases. The blue and orange bars correspond to the original and accumulated dose distributions, respectively.

sitioning variations of the lungs in relation to the ITV and differences in patient diameter, so differences between the original and accumulated dose distributions were expected. However, the differences observed in the accumulated plans are smaller than the ones observed for the plans recalculated in the extreme breathing phases. The fact that inter-fraction variability is smaller than intra-fraction variability has already been proven by Huijskens et al. (Sophie C Huijskens et al., 2017). This is due to the fact that, unlike 4D-CT that represents one full breathing cycle divided in 10 phases, CBCTs acquired during free breathing include more breathing cycles than the 4D-CT. Thus, the differences observed on the accumulated dose distribution are the consequence of a dose blur obtained not only by averaging the motion over several breathing cycles to obtain one CBCT image, but also by accumulating 8 to 10 dose distributions.

Another study by Huijskens et al. proved that respiratory-induced diaphragm motion observed in the 4D-CT acquired before treatment does not accurately predict the respiratory motion observed in the daily CBCTs (Sophie C. Huijskens et al., 2018). Thus, differences in the CBCTs are indeed expected and can even be greater than the ones observed on the extreme breathing phases of the 4D-CT. However, by comparing Huijskens' findings with the results of this study, it is possible to observe that inter-fraction changes are not as impactful on the dose distributions as the intra-fraction changes. Moreover, the hot spot values observed in the CBCTs are approximately half of those seen during the maximum lung expansion phase. Therefore, the CBCTs of patients with greater differences (patients 5, 7, 9, 16 and 19) might be depicting the inhalation phase of the breathing cycle, as the accumulated dose plans present the same tendency to increase as the plans recalculated on the maximum lung expansion phase.

Although differences are observed between the original and the accumulated dose distributions, lung ITV coverage is not compromised, nor hot spot values exceed the constraint $V_{107\%} < 10\%$.

4.2.1.2 Dose to the OARs

The results regarding average dose to the OARs are presented in Table 4.4 and the results per patient are presented in Figure 4.12. No clinically relevant differences were acknowledged between the original and accumulated dose distributions.

Although the results per patient present no clinically relevant differences between the original and the accumulated plans, there are OARs receiving more dose than the defined constraint. As the patients with dose to the OARs above the constraints are the same as in the intra-fraction study (which was expected for the original plan, but was not assumed for the accumulated plans), interpretation of the results was

Table 4.4: D_{mean} and $D_{2\%}$, in percentage, comparison between the planned and accumulated doses of patients without lung metastases. The values are represented as a percentage of the respective PD. *Abbreviations: MG = mammary glands, SD = Standard Deviation.*

Structure	Parameter	Mean ± SD (%)		Range (%)	
		Original	Accumulated	Original	Accumulated
Heart	$D_{2\%}$	100.7 ± 0.4	102.0 ± 0.4	[99.1; 103.1]	[100.5; 104.3]
Liver	D_{mean}	46.7 ± 3.3	47.4 ± 3.2	[27.3; 61.4]	[28.5; 61.6]
Spleen	D_{mean}	54.8 ± 2.7	55.4 ± 2.8	[41.7; 70.0]	[41.9; 71.0]
Left MG	D_{mean}	44.4 ± 6.7	46.9 ± 7.5	[25.5; 80.9]	[25.1; 90.5]
Right MG	D_{mean}	44.9 ± 7.8	49.1 ± 8.2	[23.5; 88.9]	[23.5; 97.5]
Thyroid	D_{mean}	13.4 ± 1.5	13.7 ± 1.6	[5.9; 10.2]	[6.3; 20.9]

performed for this same group of patients in section 4.1, "Robustness of photon dose distributions against intra-fraction anatomical changes".

Unlike the $V_{107\%}$ values of patients 7, 9, 16 and 19, OAR doses per patient do not present the same tendency to an increase in the accumulated plans. However, the dose to the mammary glands of patient 5 is the same as the one obtained for the maximum lung expansion phase, supporting the hypothesis that for some patients the lung phases in the CBCTs are more similar to the maximum lung expansion phase than to the averaged phase.

4.2.2 Patients with lung metastases

4.2.2.1 ITV coverage and hot spots of the lungs

Average coverage of patients with metastases was 96.3% ± 3.6% (range [64.1%; 100%]) for the original dose distribution and 96.6% ± 3.2% (range [67.5%; 100%]) for the accumulated dose distribution. Average $V_{107\%}$ values were 33.0% ± 8.8% (range [6.3%; 88.1%]) and 34.7% ± 9.1% (range [7.6%; 88.4%]) for the original and accumulated dose distributions, respectively.

The results per patient are represented in Figure 4.13. Lung ITV coverage was not achieved for patient 14 and $V_{107\%}$ values were above the constraint for patients 3, 6, 10, 11, 14 and 20, even though only patient 11 presented clinically relevant differences between the two dose distributions. The $V_{107\%}$ values above the constraint for this group of patients are due to the dose fall-off of the boost doses given to the metastases, as it was investigated per patient and explained in section 4.1, "Robustness of photon dose distributions against intra-fraction anatomical changes".

To assess whether the increase in $V_{107\%}$ in the accumulated plan was due to differences in ED, as it had been observed on the maximum lung expansion phase, the ED of the left lung was investigated for all fractions. Mean ED on the registered-CTs was 0.512 versus 0.509 observed in the averaged-CT. Therefore, there is an increase in ED on the registered-CTs that originates more scatter photons within the left lung's ITV. Moreover, the hot spots in each registered-CT were not always located in the same place, resulting in a spread of the $V_{107\%}$ in the accumulated dose distribution.

4.2.2.2 PTV coverage and hot spots of metastases

The metastases coverage and hot spots of each patient are represented in Table 4.5. There are some clinically relevant differences in terms of coverage, especially for metastases 1 and 2 of patient 1, metastasis 2 of patient 10 and metastases 2 and 4 of patient 14.

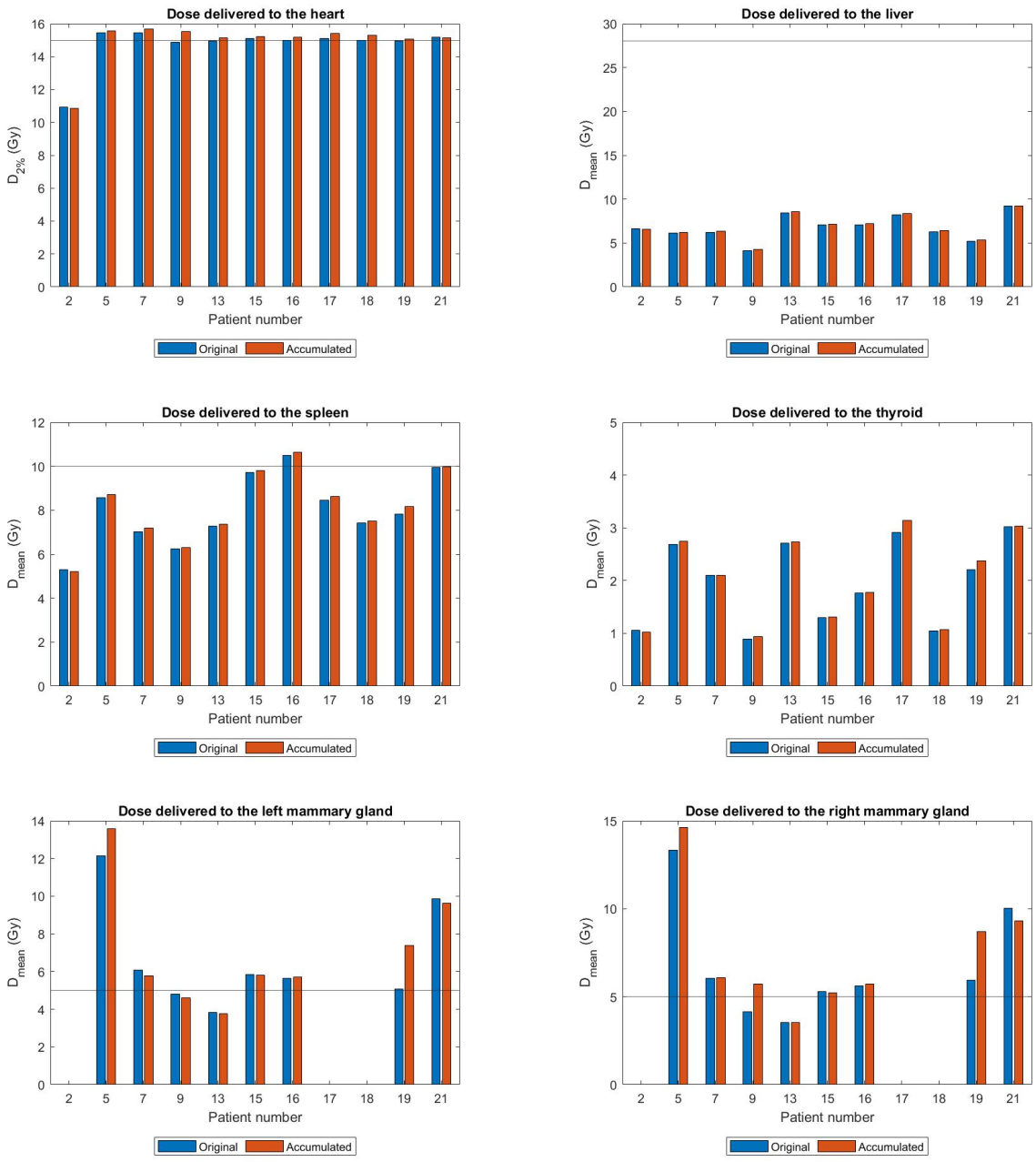

Figure 4.12: OAR dose values obtained for patients without lung metastases. The blue and orange bars correspond to the original and accumulated dose distributions, respectively, and the horizontal lines correspond to the dose constraints of each organ.

By observing the location of the lung and surrounding structures in relation to the PTV, it is observed that the PTV is covering more area outside the lung for the fractions with an increased ED, more precisely ribs (as it can be observed in Figure 4.14). However, this increase in ED results in a underdosage of metastases 1 and 2 of patient 1 and metastasis 2 of patient 10 in the accumulated plan. Since bone is a better radiation absorber compared to soft or lung tissue, the presence of part of the rib within the PTV causes an underdosage as it absorbs the radiation. This is of concern, as radiation induced fractures can occur. Conversely, metastases 2 and 4 of patient 14 present an increase in terms of coverage from the original to the accumulated plans, caused by an increase in ED.

The low PTV coverage of metastases can greatly impact treatment outcome, as there is significant

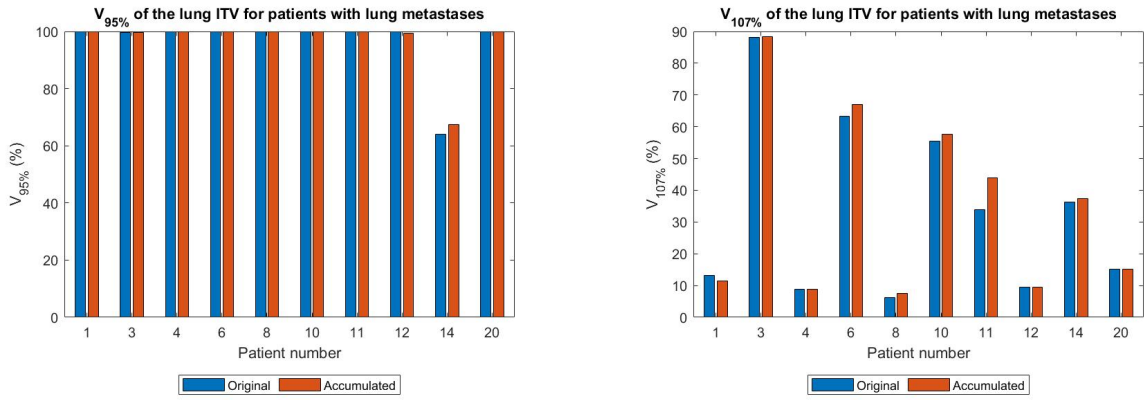

Figure 4.13: $V_{95\%}$ and $V_{107\%}$ values of the lung ITV for patients with lung metastases. The blue and orange bars correspond to the original and accumulated dose distributions, respectively.

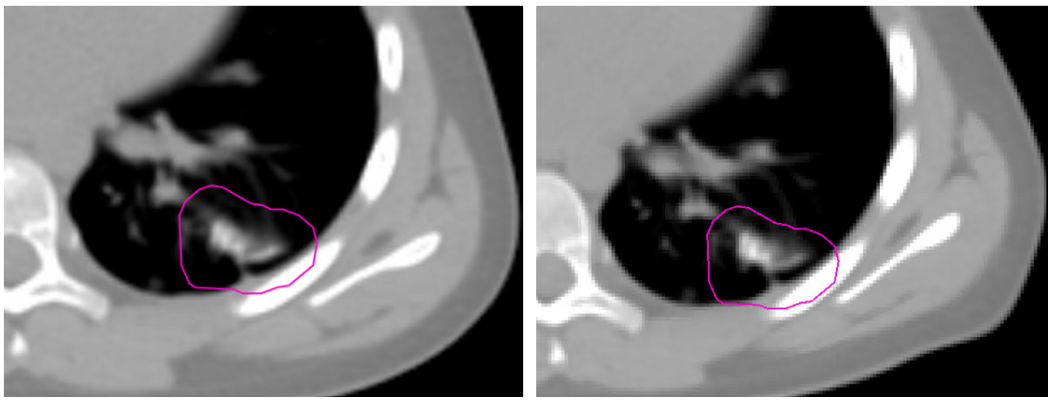

Figure 4.14: Position of the PTV of metastasis 1 of patient 1 on the averaged-CT (left) and on the registered-CT (right) for one fraction, in which it is possible to observe how in the registered-CT there is more rib volume within the PTV, resulting in an underdosage, as the rib absorbs more radiation than soft or lung tissue.

radiation being delivered, but there is still underdosage. Additionally, there is the risk that inter-fraction changes cause shifts in dose deposition, leading to a possible dose blur. This is particularly important, as there will be more lung volume receiving boost doses, but also more volume of surrounding OARs (as it was observed that the presence of boost doses affects OAR dose).

As aforementioned, CBCTs are acquired during free breathing and therefore include more breathing cycles than the 4D-CT. In practice, and considering the dose being delivered to the metastases, a dose blur would be detected not only by an underdosage of the metastases, but also by an increase in the high dose volume within the lung ITV. However, by observing the $V_{107\%}$ results, there is no evidence of a boost dose blur in the lung ITV. Additionally, ITV coverage was investigated, concluding that the constraint $V_{95\%} > 99\%$ is met for all metastases ITV included in the study. Thus, inter-fraction motion does not seem to have a significant impact on the patients' dose distributions.

4.2.2.3 Dose to the OARs

Regarding dose to the OARs, the average values are represented in Table 4.6, with no clinically relevant differences to report. However, there are noticeable differences between the original dose being evaluated on this study and the original dose presented in the intra-fraction study (see Table 4.3). These differences are approximately 4% in terms of percentage of the PD, and are explained by the different software used to retrieve the results of both studies. The software used to recalculate the original plan in

Table 4.5: Metastases PTV coverage and hot spots of the planned and accumulated dose distributions.

Patient	Boost	$V_{95\%}$ (%)		$V_{107\%}$ (%)	
		Original	Accumulated	Original	Accumulated
1	1	99.8	85.7	0	0
	2	98.3	70.5	0	0
3	1	99.7	99.9	0	0
	2	100	100	0	0
4	1	100	100	0	0
6	1L	99.9	100	0	0
	2L	95.9	98.0	0	0
	3L	99.2	99.7	0	0
	4L	97.5	100	0	0
	5L	98.5	99.7	0	0
	6L	99.6	100	0	0
	1R	96.9	99.8	0	0
	2R	96.5	99.2	0	0
	3R	97.1	99.4	0	0
	4R	98.3	99.5	0	0
	5R	95.4	99.5	0	0
	6R	97.9	100	0	0
	7R	99.3	99.8	0	0
8	1	99.8	100	0	0
10	1	99.8	96.5	0.7	0
	2	98.1	91.2	0	0.8
	3	99.5	98.2	0	0
11	1	100	99.6	0	0
	2	100	99.9	0	0
12	1	100	96.0	0	0
14	1	93.4	96.7	0	0
	2	70.2	82.9	0	0
	3	95.0	99.2	0	0
	4	89.9	99.5	0	0
	5	99.9	100	0	0
20	1	94.8	94.5	0	0

the extreme breathing phases and in the registered-CTs was Monaco treatment planning system (Elekta, Stockholm, Sweden). However, while the DVH parameters of the intra-fraction study were retrieved directly from Monaco, the DVH parameters of the inter-fraction study were retrieved from Volumetool, an in-house built delineation software (Bol et al., 2009). This difference in terms of software is not ideal and is due to the software's different uncertainties. However, fractional dose accumulation could not be performed with the Monaco treatment planning system (Elekta, Stockholm, Sweden), thus the employment of Volumetool.

The results per patient present no clinically relevant differences, and can be observed in Figure 4.15. Once again, OAR dose is above the defined constraint for most patients when considering the heart and mammary glands.

The OAR doses in the accumulated plans are similar to the doses obtained in the intra-fraction study for this subgroup of patients. This supports the hypothesis that the breathing phases represented on the

Table 4.6: D_{mean} and $D_{2\%}$, in percentage, comparison between the planned and accumulated doses of patients with lung metastases. The values are represented as a percentage of the respective PD. *Abbreviations: MG = mammary glands, SD = Standard Deviation.*

Structure	Parameter	Mean ± SD (%)		Range (%)	
		Original	Accumulated	Original	Accumulated
Heart	$D_{2\%}$	120.8 ± 5.8	120.0 ± 6.0	[99.6; 141.1]	[98.8; 141.7]
Liver	D_{mean}	51.9 ± 9.0	52.4 ± 9.1	[26.9; 98.0]	[27.1; 98.5]
Spleen	D_{mean}	51.1 ± 5.2	51.7 ± 5.3	[30.8; 88.3]	[30.3; 88.8]
Left MG	D_{mean}	48.4 ± 4.3	54.0 ± 6.3	[25.4; 74.9]	[27.1; 93.1]
Right MG	D_{mean}	49.4 ± 4.7	53.6 ± 5.6	[31.3; 77.3]	[36.7; 91.4]
Thyroid	D_{mean}	20.1 ± 2.3	20.7 ± 2.2	[7.5; 31.0]	[7.5; 28.5]

CBCTs are more similar to one of the extreme breathing phases than to the averaged phase.

The greater differences in OAR dose, although clinically irrelevant, are observed for the mammary glands. As previously mentioned, patient diameter differences were observed for several CBCTs, which led to a need to create a new body contour on which to recalculate the plan. This step was taken due to the fact that in some patients there was a considerable part of the body outside the body contour, but also due to an air gap between the body and the body contour. However, the fractional doses were rigidly accumulated, meaning that these new contours were applied when recalculating the plan, but the accumulated dose distribution was matched to the original body contour. For this reason, a dose blur on the chest was observed for some patients, which in turn affects mostly the mammary glands, as it is the most anterior OAR.

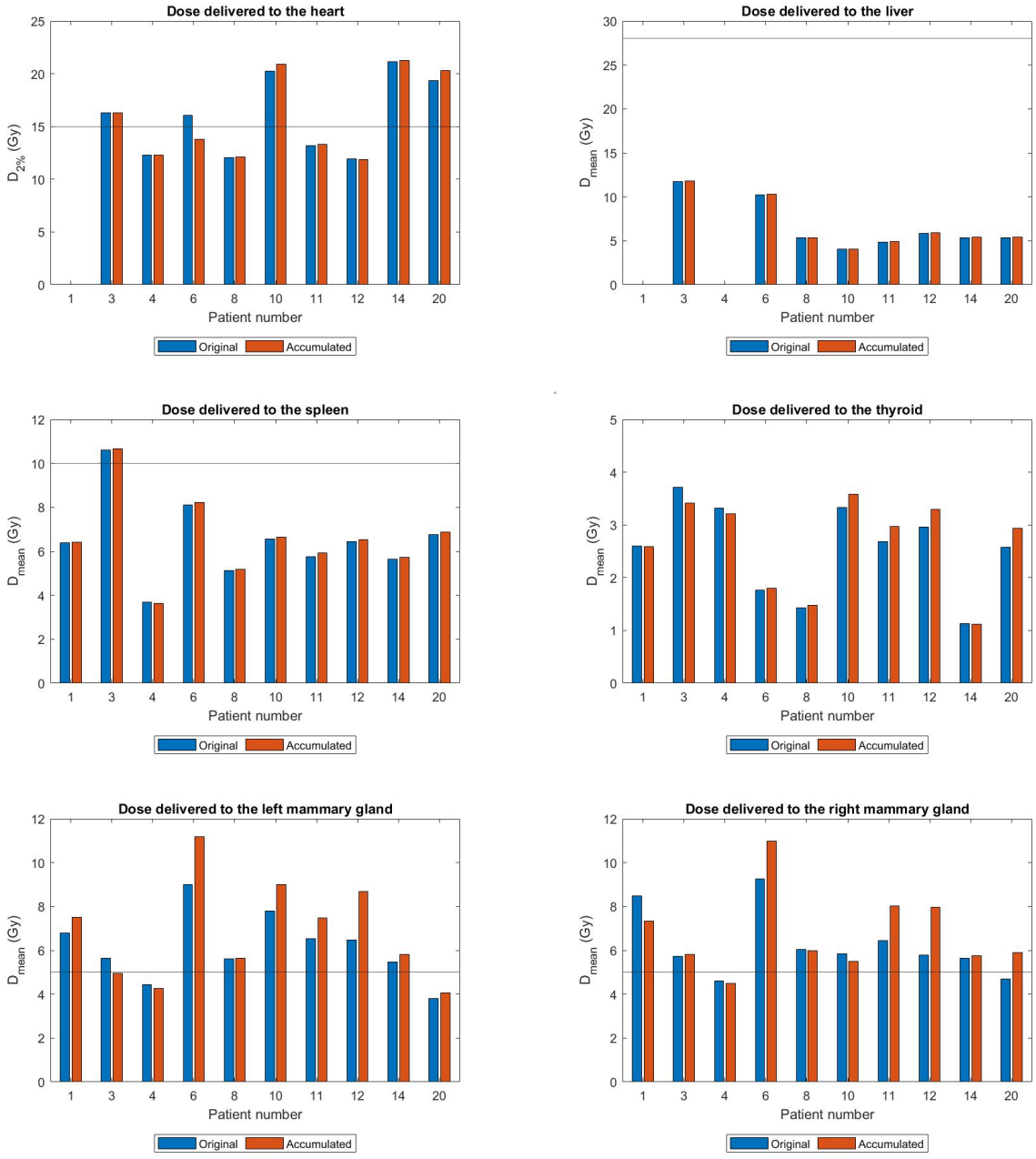

Figure 4.15: OAR dose values obtained for patients with lung metastases. The blue and orange bars correspond to the original and accumulated dose distributions, respectively, and the horizontal lines correspond to the dose constraints of each organ.

Chapter 5

Robustness of proton dose distributions against inter-fraction anatomical changes

The following chapter comprises a brief overview of proton therapy, including basic concepts and the use of proton therapy to deliver WLI, based on recently published studies. Additionally, a new method to evaluate treatment robustness is presented, which enables a better comparison between PTV-based photon therapy plans and robustly optimized plans.

This overview of proton therapy is included in this dissertation work to introduce a comparison study to be performed between photon and proton dose distributions, further explained in the section "Future Work". This comparison study is to be completed in collaboration with the University Medical Center Groningen.

5.1 Physics of proton therapy

Currently, the main advantage of proton therapy is the ability to reduce dose in normal tissues. The fact that protons travel through the body and stop abruptly at a prescribed depth, which can be precisely controlled, make proton therapy attractive for the treatment of certain tumors and patient populations, including children (Merchant et al., 2014).

Protons are positively charged particles that, depending on their energy, interact with matter through Coulomb interactions with atomic electrons, Coulomb interactions with nuclei and nuclear interactions. In the radiotherapy setting, proton energies range between 70-250 MeV which result mostly in Coulomb interactions with atomic electrons (Lomax, 2009). These electrons then travel a short distance from the proton path while ionizing and depositing energy. The rate at which protons lose their energy increases as their velocity decreases, resulting in an energy peak followed by an abrupt stop. This process of dose deposition produces a very characteristic depth-dose curve, the Bragg curve, and the point of highest dose is called the Bragg peak. The Bragg peak is what makes proton therapy such a desirable technique, as it is a function of initial energy and therefore can be predicted (Mohan et al., 2017). This results in a potentially beneficial treatment for patients, as the entrance dose is reduced and the exit dose is negligible as compared to photon treatment techniques (Langen et al., 2015).

When comparing a single monoenergetic proton beam with a photon beam, the differences are clear: there is considerably less dose being delivered to normal tissue since the proton loses most of its energy at the end of its range (see Figure 5.1). The same happens when comparing multiple proton and photon beams. Conversely, when comparing multiple proton beams and intensity-modulated photon beams, the

differences are less obvious — there may be less dose being delivered to normal tissue with the proton beams, but those differences are often very small (less than 5 Gy). Although the use of a series of weighted Bragg peaks — spread out Bragg peak (SOBP) — are used to achieve target coverage and normal tissue sparing, as observed in Figure 5.1, an irregular field is created with intensity-modulated photon beams, which conforms to the tumor shape and shields normal tissue (Merchant et al., 2014; Taylor et al., 2004). Moreover, the dose distribution might be less conformal and uniform when proton therapy is chosen, which is a consequence of the need of additional devices for collimation and distal shaping of the proton beam to match the target volume. The amount of time needed to mount and use these beam-specific devices limits the practicality of multiple beams and subsequently the conformity and uniformity of the delivered dose (Merchant et al., 2014).

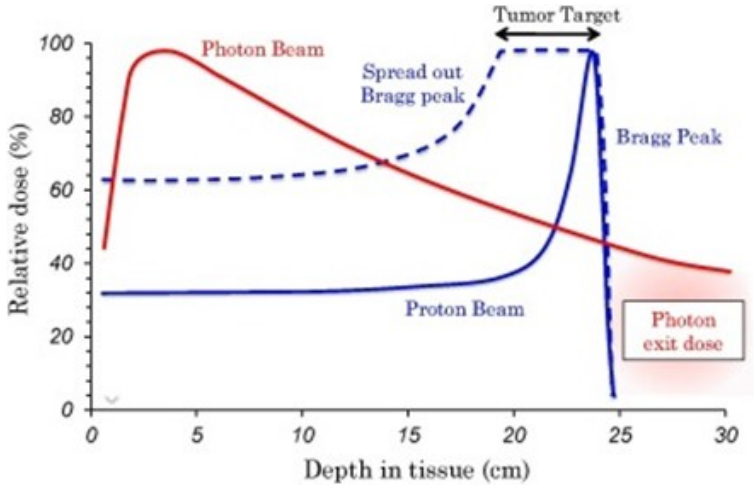

Figure 5.1: Dose deposition for a photon and proton beams, with the representation of the Bragg peak and SOBP *[adapted from (Li et al., 2020)]*.

5.2 Proton therapy for whole lung irradiation

Only recently, studies have been conducted focusing specifically on the use of proton therapy for WLI (Cunningham et al., 2020; Flampouri et al., 2021; Sha et al., 2021; Wong et al., 2021) and its comparison to existing photon techniques. In these studies, proton therapy is delivered by pencil beam scanning, in which the beams are originated in an accelerator and manipulated to treat tumors located at varying depths. This is accomplished by altering the number of protons (local dose deposition), proton energy (local penetration) and magnetic deflection (off-axis coverage). Proper target coverage and simultaneous reduction of the integral dose bath are achieved by electromagnetic control of the pencil beams (Moreno et al., 2019). In terms of beam arrangements, studies have reported the use of two posterior oblique fields (Cunningham et al., 2020), three posterior fields (Flampouri et al., 2021), anteroposterior technique (Sha et al., 2021) and anteroposterior-posteroanterior technique (Wong et al., 2021) considering the target volume as the whole lung. Additionally, the use of three beams was investigated, considering the target volume as the unilateral lung (Sha et al., 2021).

The results of the aforementioned studies suggest the feasibility of recurring to proton therapy to treat pediatric patients receiving WLI (Cunningham et al., 2020). Moreover, the dosimetric studies performed suggest significant dose reductions to the OARs when delivering IMPT, compared to VMAT and IMRT (Flampouri et al., 2021; Wong et al., 2021).

5.3 Robust treatment planning in proton therapy

The ITV and PTV margins have proven to be efficient when considering a dose distribution invariant to errors, which is an inherent fact in the PTV concept (Karlsson et al., 2017). However, when considering proton therapy, this assumption is not valid due to the relationship between the proton range and stopping power of the material that the beam is penetrating (Lomax, 2008a; Paganetti, 2012). Besides the uncertainties in predicting the stopping power, the proton range is highly influenced by patient setup or anatomy differences, leading to the need of a different method to assure treatment robustness (Lomax, 2008b). This leads to the concept of robust optimization, in which the deviations from the error-free dose distributions are calculated for different scenarios and minimized using planning objectives (Korevaar et al., 2019).

To assess whether coverage criteria have been satisfied for all the considered scenarios, a new evaluation method was proposed. This method allows comparison between PTV-based treatment plans and robustly optimized plans, especially in proton therapy (Korevaar et al., 2019). Since the plan is recalculated for a variable number of scenarios — each scenario corresponding to a shift in a different direction — a feasible method to evaluate dose distribution is to summarize all dose distributions from different scenarios into one. This summarized dose distribution calculation can then be evaluated by its voxel-wise minimum dose, which is the composite of minimum dose values per voxel from all scenarios (Lomax et al., 2004). Other alternatives include analyzing the voxel-wise mean dose (composite of the mean dose calculated per voxel from all the scenarios), or the dose distribution in the worst-case scenario - which corresponds to the scenario with worst target coverage. In Figure 5.2, these new dose evaluation methods are represented:

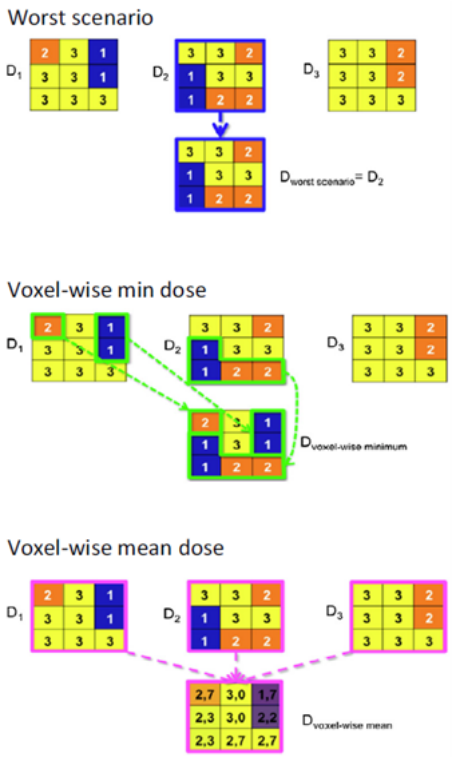

Figure 5.2: Representation of the worst scenario, voxel-wise minimum dose and voxel-wise mean dose of three scenarios *[adapted from (Korevaar et al., 2019)].*

5.4 Future work

The initial goal of this project, which was delayed by the COVID-19 pandemic, was to perform a comparison between photon and proton dose distributions against intra and inter-fraction anatomical changes. Although it will not be included in this dissertation, work towards such comparison study is already taking place in collaboration with University Medical Center Groningen.

Follow-up work on this project includes the creation of proton treatment plans, employing the Raystation software (Raysearch, Stockholm, Sweden). This proves to be a challenging step, as there are no guidelines and the literature regarding the use of proton beams to deliver WLI differs in terms of beam arrangements. The procedure to follow in the recalculation of the plans is the same as the study of robustness against inter-fraction anatomical changes, with the plans being recalculated on the registered daily CBCTs and then rigidly accumulated. Since intra-fraction anatomical changes were considered a worst-case scenario situation that would not be verifiable during treatment delivery (as the patient is breathing freely and not only with the lungs at their maximum expansion phase), the comparison between treatment techniques will not be performed against intra-fraction anatomical changes.

Regarding planning target volumes, the photon treatment plans present a 5 mm PTV margin around the patient-specific ITV. To compare the proton plans with the photon PTV-based treatment plans, the robustness optimization method is employed, with a 6 mm margin and a ±3% range uncertainty. In total, 28 dose scenarios are calculated for each patient. The information from all the scenarios is combined in a voxel-wise minimum evaluation dose by calculating the minimum dose per voxel in all scenarios (see Figure 5.2). The plans are considered robust if 99% of the lung ITV receives at least 95% of the PD ($V_{95\%}$ >99%). The evaluation of hot spot values within the target volume is performed by analyzing the dose being delivered to 1% of the volume ($D_{1\%}$) and compared with that same parameter from the photon treatment plans.

The proton treatment plans are still in the initial stages and the re-calculation of the plans on the daily CBCTs has not been performed yet. Organ sparing proves to be difficult to achieve, as small changes in the treatment parameters to meet the OAR constraints often result in underdosage of lung ITV. Literature with similar patient cohorts that focus on dosimetric comparison between photon and proton treatment techniques has proven that proton therapy is advantageous in terms of OAR sparing. Thus, more work needs to be completed to achieve clinically acceptable plans, with proper target coverage and satisfactory OAR sparing.

Chapter 6

Conclusion

Whole lung irradiation is an important component of the treatment of lung metastases that develop from solid tumors among the pediatric population. However, late toxicity that arises from the treatment is of concern, as children are more sensitive to radiation. The Childhood Cancer Survival Study showed that 5-year survivors that received chest or whole-body irradiation presented an increased risk of long-term pulmonary complications. Additionally, there is the need to consider the long-term effect in other OARs as well, such as the heart, mammary glands and thyroid, with reports of WLI leading to a higher prevalence of cardiac complications or secondary malignancies.

During treatment delivery, changes in the patient anatomy might occur. These can be observed during a single fraction, such as the breathing motion, or between fractions, such as changes in patients' positioning or diameter. To assure proper coverage, a treatment plan needs to be robust against such changes. This is accomplished by the employment of safety margins, which are advantageous in terms of target coverage, but results in the irradiation of surrounding organs.

The goal of this study was to perform a robustness study against intra and inter-fraction anatomical changes for 21 pediatric patients receiving WLI. Patients' primary tumors were mostly Wilms' tumor and Ewing sarcoma. For the purpose of the study, radiotherapy plans were recalculated in the extreme breathing phases of the respiratory cycle — maximum inhalation and exhalation — and in the daily CBCTs acquired during treatment. The recalculated plans were then compared to the original plans for each patient.

The results of the robustness assessment against intra-fraction changes demonstrated that the coverage was met in both extreme breathing phases, except for one patient, with no clinically relevant differences to report between the recalculated and the original plans. Conversely, larger differences were seen on $V_{107\%}$ values, especially the tendency for an increase when considering the maximum inhalation phase, with two patients presenting clinically relevant differences. These differences were investigated and are due to large diaphragm displacements, which in turn lead to a hot spot on the base of the lungs. However, these hot spots stay within the lung PTV and do not affect adjacent organs such as the liver or spleen. For the patients with lung metastases, high $V_{107\%}$ values within the lung ITV were related to the dose fall-off of metastases. Metastases coverage and hot spots were assessed on the PTV, which revealed that the PTV margin is not robust against intra-fraction changes, as there were cases of clinically relevant underdosages and hot spots. Most of these differences were due to ED changes within the metastases PTV, which due to their small dimensions makes them more prone to such changes. However, ITV constraints were met, proving that the patient-specific ITV margin defined is adequate.

Regarding the results of the robustness assessment against inter-fraction changes, no clinically relevant differences were reported, concluding that the accumulated plans are not affected by the inter-

fraction patient variations. Metastases coverage and hot spots presented some clinically relevant differences, also associated with ED changes within the metastases PTV. Similarly to the intra-fraction study, ITV coverage was met for all patients.

Lastly, dose to the OARs was assessed. The organs considered were the heart, mammary glands, thyroid, spleen, and liver. No clinically relevant differences were observed. Such differences were considered clinically relevant if greater than 3 Gy for all organs, independently of their dose constraint. The fact that this margin should be organ-specific was discussed, as dose constraints to the OARs vary a lot and some OARs are more important in terms of sparing than others.

Overall results demonstrate that the 21 plans analyzed in this study are robust against intra and inter-fraction anatomical changes. However, some differences were observed on the metastases coverage, which might lead to underdoses or hot spots, depending on the breathing pattern of the patient during treatment delivery. This is a limitation imposed by delivering treatment during free breathing, as the breathing motion is unpredictable. In this study it was discussed the employment of respiratory gated treatment delivery, which has been reported to be feasible in young patients, and is speculated to be advantageous to decrease the observed dose differences. This is achieved by reducing the uncertainties caused by the breathing motion. Additionally, respiratory gated treatment delivery might allow to employ smaller target margins and, therefore, deliver less dose to surrounding OARs. Another option to deliver less dose to OARs is to recur to proton beams to deliver WLI, which has been reported to be a feasible option with proper target coverage.

References

Albertini, F., E. B. Hug, and A. J. Lomax (2011). "Is it necessary to plan with safety margins for actively scanned proton therapy?" In: *Physics in Medicine and Biology* 56.14, pp. 4399–4413. ISSN: 00319155. DOI: 10.1088/0031-9155/56/14/011.

Ambrose, J and G Hounsfield (1973). "Computerized transverse axial tomography". In: *The British Journal of Radiology* 46.542, pp. 148–149. ISSN: 0007-1285. URL: http://europepmc.org/abstract/MED/4686818.

Baskar, Rajamanickam et al. (2012). "Cancer and Radiation Therapy : Current Advances and Future Directions". In: DOI: 10.7150/ijms.3635.

Bol, Gijsbert H. et al. (2009). "Simultaneous multi-modality ROI delineation in clinical practice". In: *Computer Methods and Programs in Biomedicine* 96.2, pp. 133–140. ISSN: 01692607. DOI: 10.1016/j.cmpb.2009.04.008.

Boria, Andrew J. et al. (2019). "Interplay effect of target motion and pencil-beam scanning in proton therapy for pediatric patients". In: *International Journal of Particle Therapy* 5.2, pp. 1–10. ISSN: 23315180. DOI: 10.14338/IJPT-17-00030.1.

Bosarge, Christina L. et al. (2016). "A dosimetric comparison of whole-lung treatment techniques in the pediatric population". In: *Medical Dosimetry* 41.2, pp. 126–130. ISSN: 18734022. DOI: 10.1016/j.meddos.2015.10.006. URL: http://dx.doi.org/10.1016/j.meddos.2015.10.006.

Brock, Kristy K (2007). "Image registration in intensity- modulated, image-guided and stereotactic body radiation therapy." eng. In: *Frontiers of Radiation Therapy and Oncology* 40, pp. 94–115. ISSN: 0071-9676 (Print). DOI: 10.1159/000106030.

Burnet, N G et al. (2018). "Target volume concepts in radiotherapy and their implications for imaging". ger. In: *Der Radiologe* 58.8, pp. 708–721. ISSN: 1432-2102 (Electronic). DOI: 10.1007/s00117-018-0420-6.

Cho, B. C.John et al. (2002). "The effect of set-up uncertainties, contour changes, and tissue inhomogeneities on target dose-volume histograms". In: *Medical Physics* 29.10, pp. 2305–2318. ISSN: 00942405. DOI: 10.1118/1.1508800.

Court, L. E. (2014). *In-Room Image-Guided Radiation Therapy*. Vol. 9. Elsevier B.V., pp. 401–430. ISBN: 9780444536327. DOI: 10.1016/B978-0-444-53632-7.00924-2. URL: http://dx.doi.org/10.1016/B978-0-444-53632-7.00924-2.

Cunningham, D. et al. (2020). "Proton Whole Lung Radiation Therapy: Initial Report of Outcomes". In: *International Journal of Radiation Oncology, Biology, Physics* 108.3, e248. ISSN: 03603016. DOI: 10.1016/j.ijrobp.2020.07.598. URL: https://doi.org/10.1016/j.ijrobp.2020.07.598.

Demoor-Goldschmidt, C et al. (2017). "Respiratory-gated bilateral pulmonary radiotherapy for Ewing's sarcoma and nephroblastoma in children and young adults: Dosimetric and clinical feasibility stud-

ies." eng. In: *Cancer radiotherapie: Journal de la Societe Francaise de Radiotherapie Oncologique* 21.2, pp. 124–129. ISSN: 1769-6658 (Electronic). DOI: 10.1016/j.canrad.2016.11.003.

Demoor-Goldschmidt, C. et al. (2017). "Respiratory-gated bilateral pulmonary radiotherapy for Ewing's sarcoma and nephroblastoma in children and young adults: Dosimetric and clinical feasibility studies". In: *Cancer Radiotherapie* 21.2, pp. 124–129. ISSN: 17696658. DOI: 10.1016/j.canrad.2016.11.003. URL: http://dx.doi.org/10.1016/j.canrad.2016.11.003.

Denis De Senneville, B. et al. (2016). "EVolution: An edge-based variational method for non-rigid multi-modal image registration". In: *Physics in Medicine and Biology* 61.20, pp. 7377–7396. ISSN: 13616560. DOI: 10.1088/0031-9155/61/20/7377.

DenOtter, Tami D and Johanna Schubert (Jan. 2021). "Hounsfield Unit." eng. In: *StatPearls*. URL: https://www.statpearls.com/articlelibrary/viewarticle/23012/.

Flampouri, S. et al. (2021). "Pencil Beam Scanning Proton Whole Lung Irradiation for Pediatric Patients". In: *International Journal of Radiation Oncology, Biology, Physics* 111.3, e522–e523. ISSN: 03603016. DOI: 10.1016/j.ijrobp.2021.07.1428.

Flohr, T et al. (2002). "New technical developments in multislice CT, part 2: sub-millimeter 16-slice scanning and increased gantry rotation speed for cardiac imaging." eng. In: *RoFo : Fortschritte auf dem Gebiete der Rontgenstrahlen und der Nuklearmedizin* 174.8, pp. 1022–1027. ISSN: 1438-9029 (Print). DOI: 10.1055/s-2002-32930.

Fotina, Irina et al. (2012). "Feasibility of CBCT-based dose calculation: comparative analysis of HU adjustment techniques." eng. In: *Radiotherapy and oncology : journal of the European Society for Therapeutic Radiology and Oncology* 104.2, pp. 249–256. ISSN: 1879-0887 (Electronic). DOI: 10.1016/j.radonc.2012.06.007.

Fuchs, Joerg et al. (2012). "Surgical treatment of lung metastases in patients with embryonal pediatric solid tumors: An update". In: *Seminars in Pediatric Surgery* 21.1, pp. 79–87. ISSN: 10558586. DOI: 10.1053/j.sempedsurg.2011.10.008.

Goldman, Lee W (2008). "Principles of CT: multislice CT." eng. In: *Journal of Nuclear Medicine Technology* 36.2, pp. 56–57. ISSN: 0091-4916 (Print). DOI: 10.2967/jnmt.107.044826.

Gorgisyan, Jenny et al. (2017). "Impact of beam angle choice on pencil beam scanning breath-hold proton therapy for lung lesions". In: *Acta Oncologica* 56.6, pp. 853–859. ISSN: 1651226X. DOI: 10.1080/0284186X.2017.1287950.

Groh, B A et al. (2002). "A performance comparison of flat-panel imager-based MV and kV cone-beam CT." eng. In: *Medical Physics* 29.6, pp. 967–975. ISSN: 0094-2405 (Print). DOI: 10.1118/1.1477234.

Guerreiro, Filipa et al. (2018). "Intra- and inter-fraction uncertainties during IGRT for Wilms' tumor". In: *Acta Oncologica* 57.7, pp. 941–949. ISSN: 1651226X. DOI: 10.1080/0284186X.2018.1438655. URL: https://doi.org/10.1080/0284186X.2018.1438655.

Hendee, William et al. (2005). *Radiation Therapy Physics*. 3rd. John Wiley & Sons, Inc.

Hoffmann, Lone et al. (2018). "The NARLAL2 dose escalation trial: dosimetric implications of interfractional changes in organs at risk". In: *Acta Oncologica* 57.4, pp. 473–479. ISSN: 1651226X. DOI: 10.1080/0284186X.2017.1366049. URL: https://doi.org/10.1080/0284186X.2017.1366049.

Hugo, Geoffrey D. and Mihaela Rosu (2012). "Advances in 4D radiation therapy for managing respiration: Part I - 4D imaging". In: *Zeitschrift fur Medizinische Physik* 22.4, pp. 258–271. ISSN: 09393889. DOI: 10.1016/j.zemedi.2012.06.009.

Huijskens, Sophie C et al. (2017). "Magnitude and variability of respiratory-induced diaphragm motion in children during image-guided radiotherapy." eng. In: *Radiotherapy and Oncology: Journal of the European Society for Therapeutic Radiology and Oncology* 123.2, pp. 263–269. ISSN: 1879-0887 (Electronic). DOI: 10.1016/j.radonc.2017.03.016.

Huijskens, Sophie C. et al. (2018). "Predictive value of pediatric respiratory-induced diaphragm motion quantified using pre-treatment 4DCT and CBCTs". In: *Radiation Oncology* 13.1, pp. 1–9. ISSN: 1748717X. DOI: 10.1186/s13014-018-1143-6.

Hwang, Andrew B et al. (2009). "Can positron emission tomography (PET) or PET/Computed Tomography (CT) acquired in a nontreatment position be accurately registered to a head-and-neck radiotherapy planning CT?" eng. In: *International Journal of Radiation Oncology, Biology, Physics* 73.2, pp. 578–584. ISSN: 1879-355X (Electronic). DOI: 10.1016/j.ijrobp.2008.09.041.

Ichiji, Kei et al. (2013). "A Respiratory Motion Prediction Based on Time-Variant Seasonal Autoregressive Model for Real-Time Image-Guided Radiotherapy". In: *Frontiers in Radiation Oncology*. DOI: 10.5772/56554.

Johnston, M. et al. (2011). "Volumetric-modulated arc therapy in head and neck radiotherapy: A Planning comparison using simultaneous integrated boost for nasopharynx and oropharynx carcinoma". In: *Clinical Oncology* 23.8, pp. 503–511. ISSN: 09366555. DOI: 10.1016/j.clon.2011.02.002. URL: http://dx.doi.org/10.1016/j.clon.2011.02.002.

Kachelriess, M, S Ulzheimer, and W A Kalender (2000). "ECG-correlated imaging of the heart with subsecond multislice spiral CT." eng. In: *IEEE Transactions on Medical Imaging* 19.9, pp. 888–901. ISSN: 0278-0062 (Print). DOI: 10.1109/42.887837.

Kalapurakal, John A., Bryan Lee, et al. (2019). "Cardiac-Sparing Whole Lung Intensity Modulated Radiation Therapy in Children With Wilms Tumor: Final Report on Technique and Abdominal Field Matching to Maximize Normal Tissue Protection". In: *Practical Radiation Oncology* 9.1, pp. 62–73. ISSN: 18798500. DOI: 10.1016/j.prro.2018.07.005.

Kalapurakal, John A., Yunkai Zhang, et al. (2013). "Cardiac-sparing whole lung IMRT in children with lung metastasis". In: *International Journal of Radiation Oncology, Biology, Physics* 85.3, pp. 761–767. ISSN: 03603016. DOI: 10.1016/j.ijrobp.2012.05.036. URL: http://dx.doi.org/10.1016/j.ijrobp.2012.05.036.

Kannan, Sneha et al. (2017). "Organ motion in pediatric high-risk neuroblastoma patients using four-dimensional computed tomography." eng. In: *Journal of Applied Clinical Medical Physics* 18.1, pp. 107–114. ISSN: 1526-9914 (Electronic). DOI: 10.1002/acm2.12012.

Karlsson, Kristin et al. (2017). "Accuracy of the dose-shift approximation in estimating the delivered dose in SBRT of lung tumors considering setup errors and breathing motions". In: *Acta Oncologica* 56.9, pp. 1189–1196. ISSN: 0284-186X. DOI: 10.1080/0284186X.2017.1310395. URL: https://doi.org/10.1080/0284186X.2017.1310395.

Khan, F M (2003). *Physics of Radiation Therapy*. 3rd. Philadelphia: Lippincott Williams & Wilkins, p. 1138. ISBN: 0781730651. URL: https://medicalphys.files.wordpress.com/2010/12/faiz-khans-01.pdf.

Korevaar, Erik W. et al. (2019). "Practical robustness evaluation in radiotherapy – A photon and proton-proof alternative to PTV-based plan evaluation". In: *Radiotherapy and Oncology* 141, pp. 267–274. ISSN: 18790887. DOI: 10.1016/j.radonc.2019.08.005. URL: https://doi.org/10.1016/j.radonc.2019.08.005.

Kranen, Simon van et al. (2016). "Head and Neck Margin Reduction With Adaptive Radiation Therapy: Robustness of Treatment Plans Against Anatomy Changes". In: *International Journal of Radiation*

Oncology, Biology, Physics 96.3, pp. 653–660. ISSN: 1879355X. DOI: 10.1016/j.ijrobp.2016.07.011. URL: http://dx.doi.org/10.1016/j.ijrobp.2016.07.011.

Kwong, Yune et al. (2015). "Four-dimensional computed tomography (4DCT): A review of the current status and applications". In: *Journal of Medical Imaging and Radiation Oncology* 59.5, pp. 545–554. ISSN: 17549485. DOI: 10.1111/1754-9485.12326.

Lange, Jane M. et al. (2014). "Breast cancer in female survivors of wilms tumor: A report from the national wilms tumor late effects study". In: *Cancer* 120.23, pp. 3722–3730. ISSN: 10970142. DOI: 10.1002/cncr.28908.

Langen, Katja and Minesh Mehta (2015). "Proton Beam Therapy Basics". In: *Journal of the American College of Radiology* 12.11, pp. 1204–1206. ISSN: 1558349X. DOI: 10.1016/j.jacr.2015.08.002. URL: http://dx.doi.org/10.1016/j.jacr.2015.08.002.

Leoncini, E. et al. (2014). "Adult height and head and neck cancer: A pooled analysis within the INHANCE Consortium". In: *Head and Neck* 36.10, p. 1391. ISSN: 10970347. DOI: 10.1002/HED.

Lomax, A J (2008a). "Intensity modulated proton therapy and its sensitivity to treatment uncertainties 1: the potential effects of calculational uncertainties". In: *Physics in Medicine and Biology* 53.4, pp. 1027–1042. DOI: 10.1088/0031-9155/53/4/014. URL: https://doi.org/10.1088/0031-9155/53/4/014.

— (2008b). "Intensity modulated proton therapy and its sensitivity to treatment uncertainties 2: the potential effects of inter-fraction and inter-field motions". In: *Physics in Medicine and Biology* 53.4, pp. 1043–1056. DOI: 10.1088/0031-9155/53/4/015. URL: https://doi.org/10.1088/0031-9155/53/4/015.

— (2009). "Charged particle therapy: the physics of interaction." eng. In: *Cancer Journal (Sudbury, Mass.)* 15.4, pp. 285–291. ISSN: 1528-9117 (Print). DOI: 10.1097/PPO.0b013e3181af5cc7.

Lomax, A J et al. (2004). "The Clinical Potential of Intensity Modulated Proton Therapy". In: *Zeitschrift für Medizinische Physik* 14.3, pp. 147–152. ISSN: 0939-3889. DOI: https://doi.org/10.1078/0939-3889-00217. URL: https://www.sciencedirect.com/science/article/pii/S0939388915703259.

Mani, V.R.s and Arivazhagan Selvaraj (2013). "Survey of medical image registration". In: *Journal of Biomedical Engineering and Technology* 1, pp. 8–25.

Mc Parland, Neil A. (2009). "kV-Cone Beam CT as an IGRT Tool in the Treatment of Early Stage Prostate Cancer: A Literature Review". In: *Journal of Medical Imaging and Radiation Sciences* 40.1, pp. 9–14. ISSN: 19398654. DOI: 10.1016/j.jmir.2008.12.002. URL: http://dx.doi.org/10.1016/j.jmir.2008.12.002.

Merchant, Thomas E. and Jonathan B. Farr (2014). "Proton beam therapy: A fad or a new standard of care". In: *Current Opinion in Pediatrics* 26.1, pp. 3–8. ISSN: 10408703. DOI: 10.1097/MOP.0000000000000048.

Mertens, Ann C. et al. (2002). "Pulmonary complications in survivors of childhood and adolescent cancer: A report from the Childhood Cancer Survivor Study". In: *Cancer* 95.11, pp. 2431–2441. ISSN: 0008543X. DOI: 10.1002/cncr.10978.

Minniti, Giuseppe, Christy Goldsmith, and Michael Brada (2012). "Radiotherapy". In: *Handbook of Clinical Neurology*. Vol. 104. Elsevier B.V. Chap. 16. DOI: 10.1016/B978-0-444-52138-5.00016-5.

Mohan, Radhe and David Grosshans (2017). "Proton therapy - Present and future." eng. In: *Advanced drug delivery reviews* 109, pp. 26–44. ISSN: 1872-8294 (Electronic). DOI: 10.1016/j.addr.2016.11.006.

Moreno, Amy C. et al. (2019). "Intensity modulated proton therapy (IMPT) – The future of IMRT for head and neck cancer". In: *Oral Oncology* 88, pp. 66–74. ISSN: 18790593. DOI: 10.1016/j.oraloncology.2018.11.015.

Motosue, Megan S. et al. (2012). "Pulmonary function after whole lung irradiation in pediatric patients with solid malignancies". In: *Cancer* 118.5, pp. 1450–1456. ISSN: 0008543X. DOI: 10.1002/cncr.26371.

Mulrooney, Daniel A et al. (2016). "Cardiac Outcomes in Adult Survivors of Childhood Cancer Exposed to Cardiotoxic Therapy: A Cross-Sectional Study from the St. Jude Lifetime Cohort". In: *Annals of Internal Medicine* 164.2, pp. 93–101. DOI: 10.7326/M15-0424.Cardiac.

Mulrooney, Daniel A. et al. (2020). "Major cardiac events for adult survivors of childhood cancer diagnosed between 1970 and 1999: Report from the Childhood Cancer Survivor Study cohort". In: *The British Medical Journal* 368. ISSN: 17561833. DOI: 10.1136/bmj.l6794.

Nicolin, Gary et al. (2008). "Outcome After Pulmonary Radiotherapy in Wilms' Tumor Patients With Pulmonary Metastases at Diagnosis: A UK Children's Cancer Study Group, Wilms' Tumour Working Group Study". In: *International Journal of Radiation Oncology, Biology, Physics* 70.1, pp. 175–180. ISSN: 03603016. DOI: 10.1016/j.ijrobp.2007.05.053.

Nyeng, Tine Bisballe, Marianne Nordsmark, and Lone Hoffmann (2015). "Dosimetric evaluation of anatomical changes during treatment to identify criteria for adaptive radiotherapy in oesophageal cancer patients". In: *Acta Oncologica* 54.9, pp. 1467–1473. ISSN: 1651226X. DOI: 10.3109/0284186X.2015.1068449.

Paganetti, Harald (2012). "Range uncertainties in proton therapy and the role of Monte Carlo simulations". In: *Physics in Medicine and Biology* 57.11, R99–R117. DOI: 10.1088/0031-9155/57/11/r99. URL: https://doi.org/10.1088/0031-9155/57/11/r99.

Paganetti, Harald et al. (2002). "Relative biological effectiveness (RBE) values for proton beam therapy." eng. In: *International Journal of Radiation Oncology, Biology, Physics* 53.2, pp. 407–421. ISSN: 0360-3016 (Print). DOI: 10.1016/s0360-3016(02)02754-2.

Pai Panandiker, Atmaram S et al. (2012). "Novel assessment of renal motion in children as measured via four-dimensional computed tomography." eng. In: *International Journal of Radiation Oncology, Biology, Physics* 82.5, pp. 1771–1776. ISSN: 1879-355X (Electronic). DOI: 10.1016/j.ijrobp.2011.03.046.

Paulino, Arnold C et al. (2000). "Late effects in children treated with radiation therapy for Wilms' tumor". In: *International Journal of Radiation Oncology, Biology, Physics* 46.5, pp. 1239–1246. ISSN: 03603016. DOI: 10.1016/S0360-3016(99)00534-9.

Pein, F et al. (July 2004). "Cardiac abnormalities 15 years and more after adriamycin therapy in 229 childhood survivors of a solid tumour at the Institut Gustave Roussy." eng. In: *British Journal of Cancer* 91.1, pp. 37–44. ISSN: 0007-0920 (Print). DOI: 10.1038/sj.bjc.6601904.

Podgorsak, E B (2005). "External photon beams: physical aspects". In: *Radiation Oncology Physics: A Handbook for Teachers and Students*. Vienna: International Atomic Energy Agency. Chap. 6.

Purdy, James A. (2004). "Current ICRU Definitions of Volumes: Limitations and Future Directions". In: *Seminars in Radiation Oncology* 14.1, pp. 27–40. ISSN: 10534296. DOI: 10.1053/j.semradonc.2003.12.002.

Rigauts, H et al. (1990). "Initial experience with volume CT scanning." eng. In: *Journal of Computer Assisted Tomography* 14.4, pp. 675–682. ISSN: 0363-8715 (Print). DOI: 10.1097/00004728-199007000-00035.

REFERENCES

Rybicki, Frank J et al. (2008). "Initial evaluation of coronary images from 320-detector row computed tomography." eng. In: *The International Journal of Cardiovascular Imaging* 24.5, pp. 535–546. ISSN: 1569-5794 (Print). DOI: 10.1007/s10554-008-9308-2.

Sha, Xue et al. (2021). "A New Proton Therapy Solution Provides Superior Cardiac Sparing Compared With Photon Therapy in Whole Lung Irradiation for Pediatric Tumor Patients". In: *Frontiers in Oncology* 10, pp. 1–9. ISSN: 2234943X. DOI: 10.3389/fonc.2020.611514.

Spector, Logan G., Nathan Pankratz, and Erin L. Marcotte (2015). "Genetic and nongenetic risk factors for childhood cancer". In: *Pediatric Clinics of North America* 62.1, pp. 11–25. ISSN: 15578240. DOI: 10.1016/j.pcl.2014.09.013.

Srnivasan, Kavitha, Mohammad Mohammadi, and Justin Shepherd (2014). "Applications of linac-mounted kilovoltage Cone-beam Computed Tomography in modern radiation therapy: A review". In: *Polish Journal of Radiology* 79, pp. 181–193. ISSN: 18990967. DOI: 10.12659/PJR.890745.

Steinmeier, T., S. Schulze Schleithoff, and B. Timmermann (2019). "Evolving Radiotherapy Techniques in Paediatric Oncology". In: *Clinical Oncology* 31.3, pp. 142–150. ISSN: 14332981. DOI: 10.1016/j.clon.2018.12.005. URL: https://doi.org/10.1016/j.clon.2018.12.005.

Steliarova-Foucher, Eva et al. (2017). "International incidence of childhood cancer, 2001–10: a population-based registry study". In: *The Lancet Oncology* 18.6, pp. 719–731. ISSN: 14745488. DOI: 10.1016/S1470-2045(17)30186-9.

Stock, Markus et al. (2009). "Image quality and stability of image-guided radiotherapy (IGRT) devices: A comparative study." eng. In: *Radiotherapy and Oncology: Journal of the European Society for Therapeutic Radiology and Oncology* 93.1, pp. 1–7. ISSN: 1879-0887 (Electronic). DOI: 10.1016/j.radonc.2009.07.012.

Taguchi, K and H Aradate (1998). "Algorithm for image reconstruction in multi-slice helical CT." eng. In: *Medical Physics* 25.4, pp. 550–561. ISSN: 0094-2405 (Print). DOI: 10.1118/1.598230.

Taguchi, Katsuyuki (2003). "Temporal resolution and the evaluation of candidate algorithms for four-dimensional CT". In: *Medical physics* 30.4, pp. 640–650. ISSN: 0094-2405. DOI: 10.1118/1.1561286. URL: https://doi.org/10.1118/1.1561286.

Taylor, A. and M. E.B. Powell (2004). "Intensity-modulated radiotherapy - What is it?" In: *Cancer Imaging* 4.2, pp. 68–73. ISSN: 14707330. DOI: 10.1102/1470-7330.2004.0003.

Teoh, May et al. (2011). "Volumetric modulated arc therapy: A review of current literature and clinical use in practice". In: *British Journal of Radiology* 84.1007, pp. 967–996. ISSN: 00071285. DOI: 10.1259/bjr/22373346.

Tezcanli, Evrim Kadriye et al. (2011). "Does radiotherapy planning without breath control compensate intra-fraction heart and its compartments' movement?" In: *Breast Cancer Research and Treatment* 126.1, pp. 85–92. ISSN: 01676806. DOI: 10.1007/s10549-010-1306-0.

Tsunashima, Y (2012). "Verification of the clinical implementation of the respiratory gated beam delivery technique with synchrotron-based proton irradiation". In: *University of Texas*. URL: http://digitalcommons.library.tmc.edu/utgsbs_dissertations/267/.

Uh, Jinsoo et al. (2017). "Quantification of Pediatric Abdominal Organ Motion With a 4-Dimensional Magnetic Resonance Imaging Method." eng. In: *International Journal of Radiation Oncology, Biology, Physics* 99.1, pp. 227–237. ISSN: 1879-355X (Electronic). DOI: 10.1016/j.ijrobp.2017.05.026.

Unkelbach, Jan et al. (2018). "Robust radiotherapy planning." eng. In: *Physics in Medicine and Biology* 63.22, 22TR02. ISSN: 1361-6560 (Electronic). DOI: 10.1088/1361-6560/aae659.

Van Herk, Marcel (2004). "Errors and Margins in Radiotherapy". In: *Seminars in Radiation Oncology* 14.1, pp. 52–64. ISSN: 10534296. DOI: 10.1053/j.semradonc.2003.10.003.

Vedam, S S et al. (2003). "Acquiring a four-dimensional computed tomography dataset using an external respiratory signal." eng. In: *Physics in Medicine and Biology* 48.1, pp. 45–62. ISSN: 0031-9155 (Print). DOI: 10.1088/0031-9155/48/1/304.

Wong, Ru Xin et al. (2021). "Cardiac-sparing and breast-sparing whole lung irradiation using intensity-modulated proton therapy". In: *International Journal of Particle Therapy* 7.4, pp. 65–73. ISSN: 23315180. DOI: 10.14338/IJPT-20-00079.1.

Yahalom, Joachim et al. (2015). "Modern radiation therapy for extranodal lymphomas: field and dose guidelines from the International Lymphoma Radiation Oncology Group." eng. In: *International Journal of Radiation Oncology, Biology, Physics* 92.1, pp. 11–31. ISSN: 1879-355X (Electronic). DOI: 10.1016/j.ijrobp.2015.01.009.

Zachiu, Cornel et al. (2017). "Non-rigid CT/CBCT to CBCT registration for online external beam radiotherapy guidance." eng. In: *Physics in Medicine and Biology* 63.1, p. 15027. ISSN: 1361-6560 (Electronic). DOI: 10.1088/1361-6560/aa990e.